THE JOURNAL OF PHYSICAL CHEMISTRY A

Article

Porphyrin##-Oligo-Ethynylenephenylene#[60]Fullerene Triads: Synthesis and Electrochemical and Photophysical Characterization of the New Porphyrin#Oligo-PPE#[60]Fullerene Systems

Angelo Lembo, Pietro Tagliatesta, Dirk M. Guldi, Mateusz Wielopolski, and Marzia Nuccetelli

J. Phys. Chem. A, **2009**, 113 (9), 1779-1793• DOI: 10.1021/jp809557e • Publication Date (Web): 05 February 2009

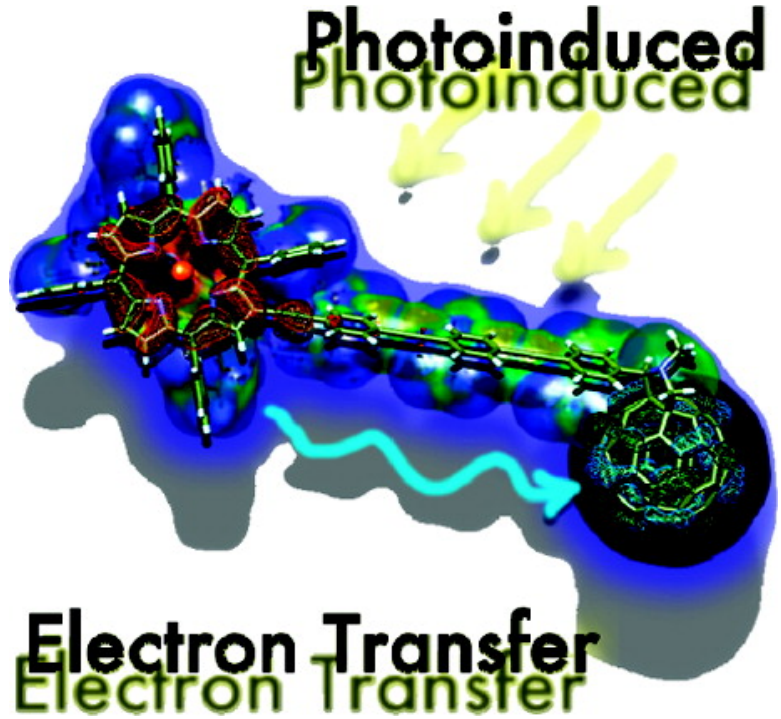

More About This Article

Additional resources and features associated with this article are available within the HTML version:

- Supporting Information
- Access to high resolution figures
- Links to articles and content related to this article
- Copyright permission to reproduce figures and/or text from this article

The Journal of Physical Chemistry A is published by the American Chemical Society. 1155 Sixteenth Street N.W., Washington, DC 20036

Porphyrin−β-Oligo-Ethynylenephenylene−[60]Fullerene Triads: Synthesis and Electrochemical and Photophysical Characterization of the New Porphyrin−Oligo-PPE−[60]Fullerene Systems

Angelo Lembo,[†] Pietro Tagliatesta,*[,†] Dirk M. Guldi,*[,‡] Mateusz Wielopolski,[‡] and Marzia Nuccetelli[§]

Dipartimento di Scienze e Tecnologie Chimiche, University of Rome "Tor Vergata", Via della Ricerca Scientifica, 00133 Rome, Italy, Department of Chemistry and Pharmacy, Friedrich-Alexander University Erlangen-Nuremberg, Egerlandstrasse 3, 91058 Erlangen, Germany, and Dipartimento di Medicina Interna, University of Rome "Tor Vergata", Via della Ricerca Scientifica, 00133 Rome, Italy

Received: October 29, 2008; Revised Manuscript Received: December 17, 2008

The synthesis and electrochemical and photophysical studies of new electron donor−acceptor arrays, bearing porphyrins covalently linked to fullerene, are described. In the reported investigation, phenyleneethynylene subunits were chosen as a linking bridge to guarantee a high conjugation degree between the donor (i.e., porphyrin), the molecular bridge (i.e., oligo-phenyleneethynylenes), and the acceptor (i.e., fullerene). To enhance the electronic interactions through the extended π-system, the molecular bridge has been directly linked to the β-pyrrole position of the porphyrin ring, generating a new example of donor−bridge−acceptor systems where, for the first time, the *meso*-phenyl ring of the macrocycle is not used to hold the "bridge" between porphyrin and fullerene moieties. This modification allows altering the chemical and physical properties of the tetrapyrrole ring. Steady-state and time-resolved fluorescence studies together with transient absorption measurements reveal that in nonpolar media (i.e., toluene) transduction of singlet excited-state energy governs the excited-state deactivation, whereas in polar media (i.e., tetrahydrofuran) charge transfer prevails generating a long-lived radical ion pair state. The lifetimes hereof range from 300 to 700 ns. The study also sheds light onto the wirelike behavior of the oligo-phenyleneethynylene bridges, for which a damping factor (β) of 0.11 ± 0.05 $Å^{-1}$ has been determined in the current study.

Introduction

Organic materials for electronic and photonic applications are under continuous and fervent studies. Great interest has been focused on the design and synthesis of molecular materials on the nanoscale size to produce novel electron donor−acceptor systems, in which charge transfer is realized over distances comparable to those known in natural photosystems. Such systems harvest solar energy in order to shuttle charges along distances of approximately 35 Å at *remarkable rates*—in a few picoseconds[1]—and with *impressive efficiencies*—nearly quantitative quantum yields.[2] In this context, the focal point is on molecular structures capable of mediating charges between the donor and the acceptor moieties. These offer, for example, the opportunity to control charge transfer/shifts over nanometer distances. An imperative requirement that these molecular structures must fulfill is an effective wirelike behavior.[3] A more practical figure of merit is the attenuation factor (β), which assists in correlating the charge-transfer rate constants with distance.[4] In fact, β should be as low as possible to facilitate fast and efficient charge transport between the donor and the acceptor sites.[5]

To this purpose, many π-conjugated organic bridges were investigated and tested as molecular wires including oligo-phenylenevinylene,[6] oligo-phenyleneethynylenes,[7] oligo-acetylenes,[8] oligo-thiophenes,[9] and oligo-phenylenes.[10] Similarly, porphyrin oligomers have also been considered as molecular wires.[11] In all these cases the wirelike behavior—efficient or inefficient—depends on the combination of several factors including the degree of conjugation in the bridge, orbital matching, donor−bridge energy gap, etc.[12] The β values that have been reported so far for the different molecular bridges range from rather low, i.e., around 0.4 $Å^{-1}$,[10d] to exceptionally small with a value of 0.01 $Å^{-1}$.[6b] As a comparison the corresponding value for vacuum is 1.0 $Å^{-1}$.

In this investigation we focused our attention on the oligo-*p*-phenyleneethynylenes (oligo-PPEs) as molecular bridges, because of their synthetic versatility and their outstanding physicochemical properties. It has been previously reported that these molecules assist in a good conduction of the charges due to their high electron density and the extended π-system.[13] In particular, as soon as these systems are self-assembled on metal surfaces (i.e., gold surface) they are able to transport and store negative charges via localized molecular orbitals.[14] Another important feature of oligo-PPEs, namely, their extended π-conjugation, guarantees reasonable contacts—over intermediate and/or long distances—between one electron donor and one electron acceptor moiety covalently linked to the two termini of the oligomer.[15]

In the newly synthesized systems, the β-pyrrole position affords the chemical junction between the bridge and the tetrapyrrole macrocycle. A carbon−carbon triple bond is chosen to afford a completely extended π−π conjugation, which starts

* To whom correspondence should be addressed. Fax: +39-06-72594754 (P.T.). E-mail: pietro.tagliatesta@uniroma2.it (P.T.); dirk.guldi@chemie.uni-erlangen.de. (D.M.G.).

[†] Dipartimento di Scienze e Tecnologie Chimiche, University of Rome "Tor Vergata".

[‡] Friedrich-Alexander University Erlangen-Nuremberg.

[§] Dipartimento di Medicina Interna, University of Rome "Tor Vergata".

10.1021/jp809557e CCC: $40.75
Published on Web 02/05/2009

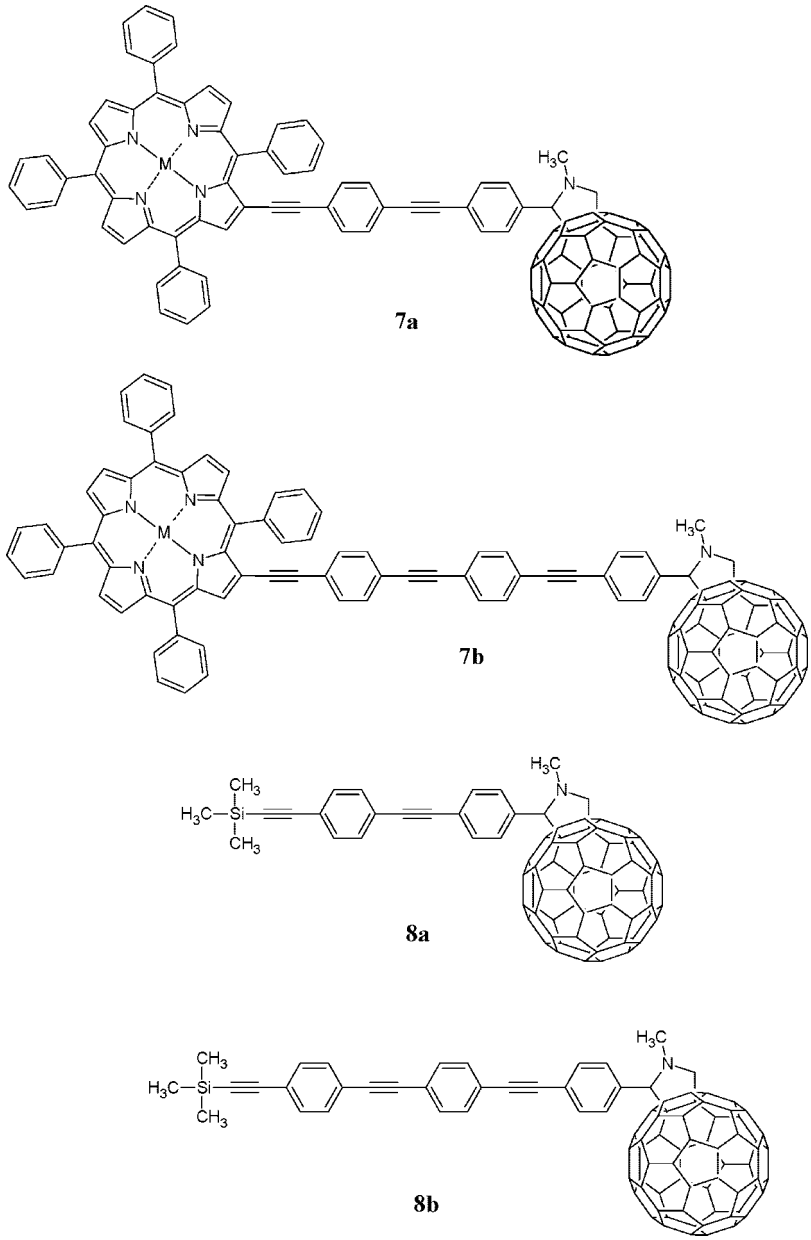

Figure 1. Porphyrin−oligo-PPE−fullerene systems and related oligo-PPE−fullerene reference compounds studied in this work. M = 2H, Zn.

on the porphyrin residue and ends in close proximity to the fullerene network, where, nevertheless, the sp^3 carbon of the pyrrolidine ring interrupts the conjugation pathway—see Figure 1.

Owing to the direct connection of the triple bond and the β-pyrrole position, charges (i.e., electrons) will be conducted through the bridge toward the electron-accepting fullerene. Implicit is a dependency on the conformation of the bridge itself. A completely planar configuration, for example, might lead to an excellent wirelike behavior, whereas a rearrangement of the phenyl rings of the bridge in an orthogonal fashion would certainly weaken the wirelike behavior.[5b,12] In fact, such a conformation might perturb the $\pi-\pi$ conjugation between the single subunits of the molecular bridge. Equally important is the matching of the orbital energy levels of the single components, which in such a case facilitate the electron transfer through the bridge enabling a charge-hopping mechanism. Alternatively the photoinduced charge-separation process may be governed by a superexchange mechanism.

In view of previously studied, similar *ex*TTF−oligo-PPE−C_{60} systems,[7e,f] the influence of the exchanging the *ex*TTF donor moiety by a porphyrin donor on the electron-transfer properties was of particular interest.

To gain thorough insight into the reaction pathway—starting with photoexcitation—both free-base porphyrin and the corresponding zinc complex were studied—see Figure 1.

Absorption measurements, cyclic voltammetry, fluorescence, and transient absorption measurements were employed to elucidate the different energy and electron-transfer reactions both in nonpolar and in polar solvents.

Results and Discussion

Synthesis. In order to gather deeper insight into the electronic interaction between the single components in the molecular triads, the reference compounds **8a**,**b**, reported in Figure 1, and **6a**,**b**, reported in Supporting Information Figure S1, were also synthesized, while the oligomers **4a**,**d** (see Supporting Informa-

SCHEME 1: Synthesis of 4-(Trimethylsilylyethynyl)benzaldehyde (1) and 1-Iodo-4-(trimethylsilylethynyl)benzene (2)

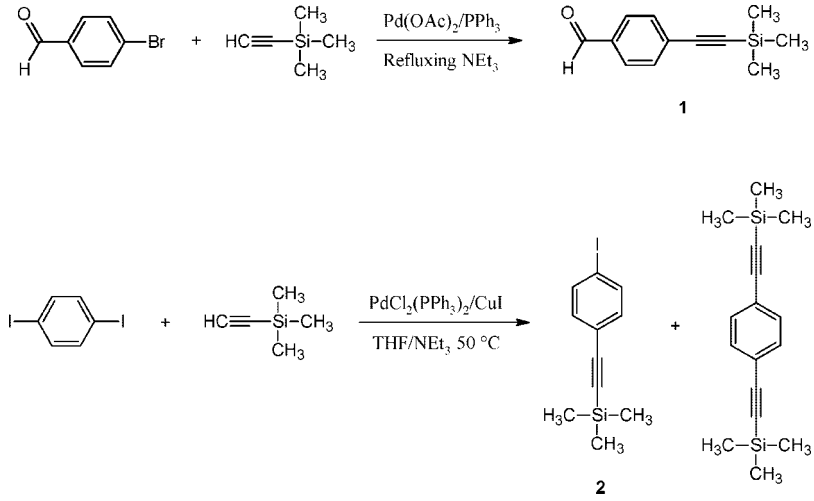

SCHEME 2: Synthesis of Different Molecular Bridges[a]

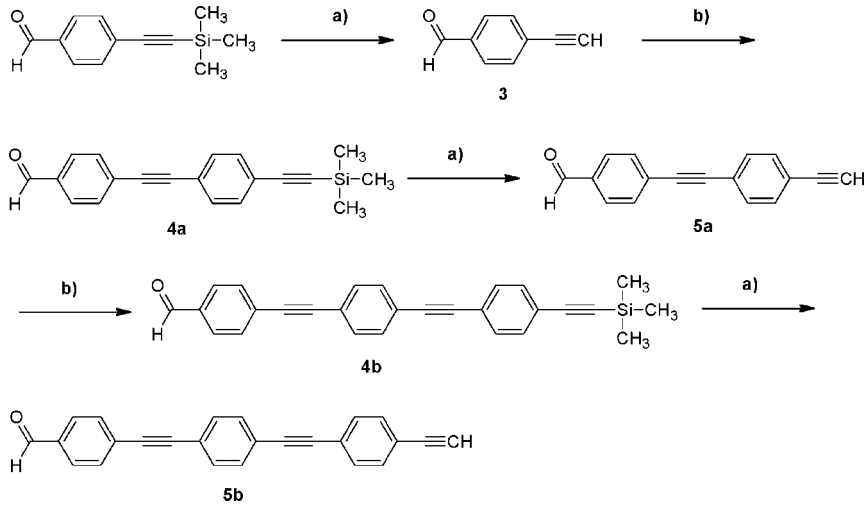

[a] (a) K_2CO_3 in $CH_3OH/CHCl_3$ solution; (b) **2**, $PdCl_2(PPh_3)_2$/CuI in THF/NEt_3 50 °C.

tion Figure S1) were used as model "wires" in the present investigation.

The first step of the synthetic procedure to obtain **7a**,**b** consisted of the synthesis of the molecular bridges with variable length. The well-known Sonogashira coupling emerged as a suitable method for obtaining the desired compounds.[16] However, in the current context it was necessary to endow the molecular "wires" with formyl groups at one of their ends to use them in the Prato reaction with C_{60}.[17] Following the synthesis of 4-(trimethylsilylethynyl)benzaldehyde[18] and 1-iodo-4-(trimethylsilylethynyl)benzene[19] (Scheme 1) it became necessary to adopt a stepwise procedure for obtaining the appropriate oligomers (Scheme 2). In particular, the synthesis of 1-iodo-4-(trimethylsilylethynyl)benzene was carried out in the presence of a slight excess of 1,4-diiodobenzene, 1.6:1, compared to trimethylsilylacetylene. This last precaution promotes the exclusive formation of the monocoupling product. Trimethylsilylacetylene was added dropwise over a period of 1 h, giving a 62% yield of the desired compound after silica gel column purification, i.e., the separation from the bis-coupling adduct.

The sequence of quantitative deprotection of the terminal ethynyl group—carried out using K_2CO_3 in $CH_3OH/CHCl_3$ solution—and subsequent condensation reaction led to the oligomers bearing either two or three ethynylenephenylene subunits (Scheme 2). ^{1}H NMR spectroscopy of **4a** and **4b** reveals the presence of two well-resolved doublets. Such resonances are due to the protons in ortho position to the aldehydic group ($\delta = 7.90$ ppm) and the terminal-protected triple bond ($\delta = 7.70$ ppm). The inner protons, on the other hand, give rise to unresolved signals. **4a** shows signals that correspond to the protons in ortho position relative to the internal triple bond as an unresolved double doublet ($\delta = 7.50$ ppm). In **4b**, the two and four protons as part of the inner phenyl rings and of those in ortho position with respect to the two internal triple bonds, respectively, are evidenced as two slightly broadened singlets ($\delta = 7.55$ and 7.48 ppm).

The synthetic pathway for obtaining **6a**,**b**, and **7a**,**b**, as reported in Scheme 3, involved the terminally deprotected triple bond compounds **5a** and **5b**. The use of the catalytic system $Pd(dba)_2/AsPh_3$ in the coupling reaction between the bromoporphyrin and the terminal alkyne compounds afforded the desired products in good yields (65−70%).

Despite the tetrapyrrole ring asymmetry, the ^{1}H NMR analysis reveals a quite simple β-pyrrole proton pattern for both porphyrin−oligo-PPE systems (**6a** and **6b**): one singlet (1H) at $\delta = 9.10$ ppm corresponding to the proton of the substituted pyrrole, two singlets (each one 2H) at $\delta = 8.90$ and 8.70 ppm due to the protons on the two remaining pyrrole rings, one adjacent and the other one opposite to the substituted pyrrole and two doublets (each one 1H) at $\delta = 8.85$ and 8.77 ppm

SCHEME 3: Synthesis of 6a,b and 7a,b Systems

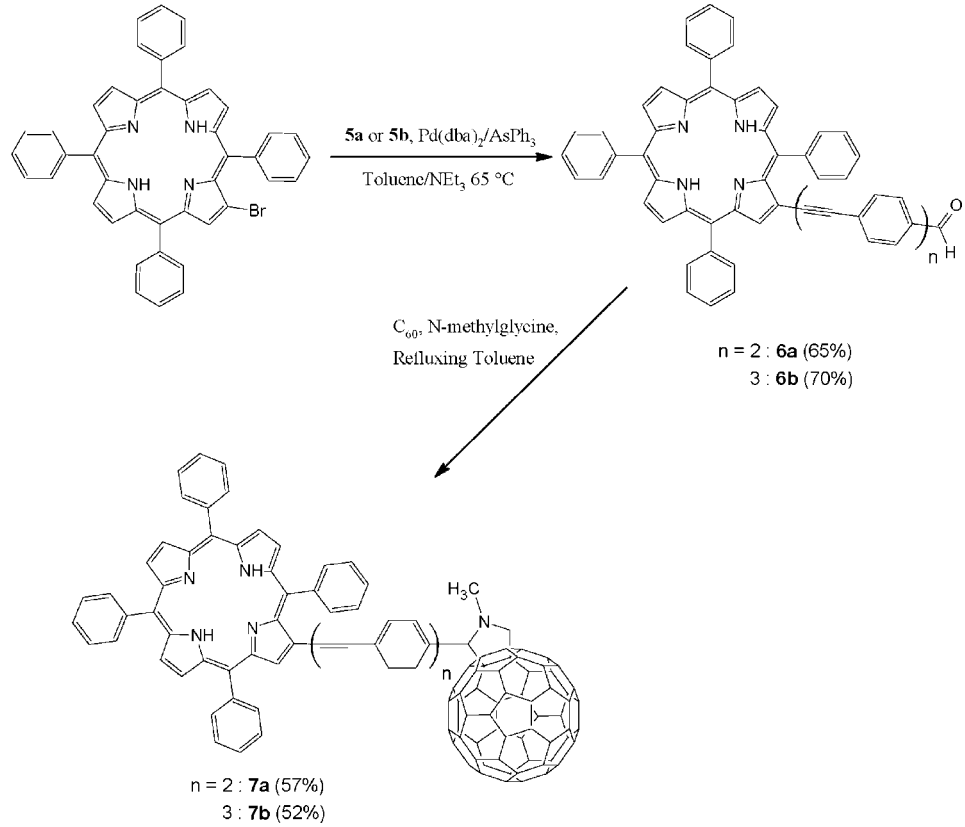

arising from the fourth pyrrole ring adjacent to the substituted ones.[20] The compounds **4a** and **4b** together with **6a** and **6b**, were subsequently used for the cycloaddition reaction with fullerene, affording, respectively, the reference compounds **8a** and **8b** (see Figure 1) and the desired ZnP/H_2P systems **7a** and **7b**.

In the ^{1}H NMR analysis, all the fulleropyrrolidine derivatives exhibit the typical proton pattern of 2-substituted pyrrolidines. In particular, two doublets at $\delta = 4.90$ and 4.13 ppm, originating from the methylene protons, one singlet at $\delta = 4.80$ ppm, due to the hydrogen in the position two of pyrrolidinic ring, and finally one additional singlet at $\delta = 2.80$ ppm, arising from the methyl substituent on the nitrogen atom.

Finally, the respective zinc(II) porphyrinate complexes of all compounds **6a**,**b** and **7a**,**b** were obtained following the well-known procedure for the zinc insertion. A saturated solution of $Zn(OAc)_2$ was added dropwise to a chloroform solution of the desired compound, and the resulting mixture was left to react at room temperature for 2 h. After that the zinc complex was recovered by filtration through a silica gel plug eluted with chloroform. The matrix-assisted laser desorption ionization time-of-flight (MALDI-TOF) analysis of ZnP/H_2P **7a**,**b** confirms the presence of the molecular peaks for both compounds at $[m/z]^+ = 1589$ uma for **7a** and $[m/z]^+ = 1689$ uma for **7b** with M = 2H and at $[m/z]^+ = 1652$ uma and $[m/z]^+ = 1752$ uma, respectively, for **Zn7a** and **Zn7b** with M = Zn. All the reported compounds were characterized by ^{1}H NMR, mass spectrometry (MS), and UV−vis analysis.

UV−Vis Study. The UV−vis spectra of all compounds were recorded in toluene. **4a** exhibits two distinct peaks at 325 and 347 nm, whereas **4b** shows a broadened, red-shifted and less defined absorption band with a maximum at 345 nm due to the extended conjugation arising from the insertion of an additional ethynylenephenylene subunit (Supporting Information Figure S2).

The absorption spectra of **8a**,**b** attest a blue shift of the absorption bands relative to **4a**,**b**. This trend is ascribed to the loss of aldehyde groups upon functionalization with C_{60}. A reduction of the conjugation length is implicit as it may arise due to the introduction of sp^3 carbon atom at the termini of the wires. In addition, the fullerene absorption, which enters into the visible region, is clearly discernible (Figure 2).

A comparison of the UV−vis spectra of the ZnP and H_2P derivatives of **7a**,**b** to those of the other reference compounds, namely, the oligo-PPE−C_{60} reference compounds **8a**,**b** and porphyrin−oligo-PPE systems **6a**,**b**, reveals a lack of appreciable electronic interactions in the ground state. The Soret bands of ZnP and H_2P, for example, remain fixed at 436 and 430 nm, respectively, even upon functionalization with C_{60} (Figure 2).

Cyclic Voltammetry Studies. The electrochemical characterization of the compounds was carried out at room temperature in a 0.05 M tetra-*n*-butylammonium hexafluorophosphate ($TBAPF_6$) *o*-dichlorobenzene (*o*-DCB) solution, using a saturated calomel electrode (SCE) as reference electrode, a platinum button working electrode, and a platinum wire counter electrode. **4a**,**b** reveal in the investigated electrochemical window, i.e., between −2.0 and 1.8 V, only a single but irreversible reduction peak at −1.75 V. However, no particular oxidation processes are visible.[21] For **8a**,**b**, on the other hand, three reduction processes are discernible in the potential range between −2.25 and 0 V. These three reduction steps occur for **8a** at −0.64, −1.10, and −1.70 V, whereas in **8b** slightly shifts toward less negative potentials (i.e., −0.62, −1.06, and −1.65 V) are present.

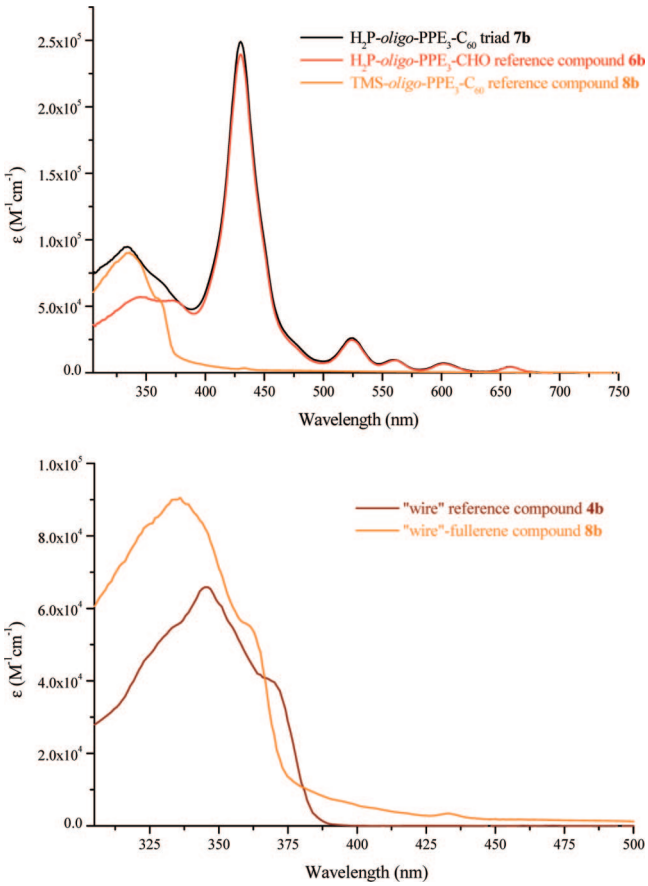

Figure 2. UV−vis absorption spectra of compounds **6b**, **7b**, and **8b** in toluene solution (n = 3) with M = 2H (upper part). UV−vis absorption spectra of compounds **4b** and **8b** in toluene solution (n = 3) (lower part).

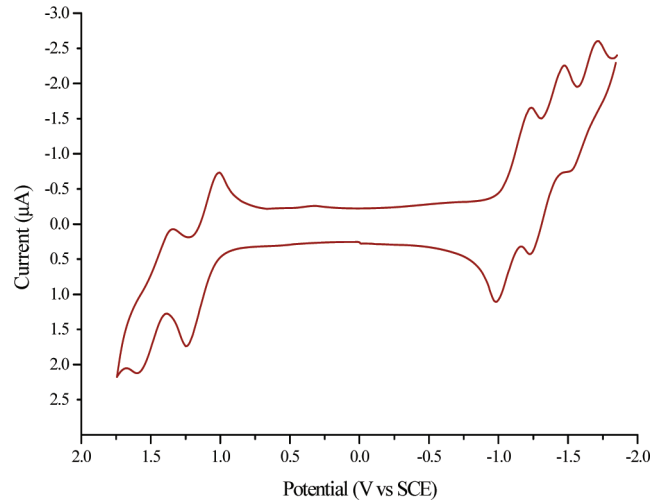

Figure 3. Complete scan of **6b** in *o*-DCB solution with 0.05 M $TBAPF_6$.

TABLE 1: Oxidation and Reduction Potentials in DCB Solution, with 0.05 M $TBAPF_6$, for the Investigated Compounds

	oxidation (V)		reduction (V)			
compd	I	II	I	II	III	IV
6a	1.12	1.45	−1.10	−1.33	−1.74[a]	
4a					−1.74[a]	
Zn6a	0.96	1.26	−1.31[b]	−1.47[b]	−1.87[b]	
8a			−0.64	−1.10	−1.70	
7a	1.10	1.46	−0.63	−1.09	−1.39	−1.63
Zn7a	0.96	1.23	−0.63	−1.02	−1.30	−1.59
6b	1.11	1.45	−1.10	−1.34	−1.60	
4b					−1.76[a]	
Zn6b	0.98	1.28	−1.30	−1.59		
8b			−0.62	−1.06	−1.65	
7b	1.20[c]	1.52[c]	−0.65	−1.08	−1.34	−1.59
Zn7b	0.98	1.24	−0.64	−1.02	−1.31	−1.58

[a] Irreversible. [b] Potential values obtained by square wave voltammetry. [c] Values corresponding to the oxidation wave vertex.

However, the differences of 20, 40, and 50 mV for the first, second, and third reduction process, respectively, are not sufficient to propose electronic interactions between the electroactive units. **6a** and **6b** give rise to a pattern that is typically found in the electrochemistry of porphyrins. In particular, two oxidation steps between 1 and 1.5 V, two reduction steps between −1 and −1.35 V, plus one irreversible reduction step at −1.75 V, are seen. The latter is, nevertheless, due to the oligomer−aldehyde functionality (Figure 3).

In the cyclic voltammograms of **7a** and **7b** the redox processes for all the subunits (i.e., H_2P, oligo-PPE, and C_{60}) are detected. The two oxidation processes are associated exclusively with H_2P, whereas the four reduction processes are spread over H_2P and C_{60}. One of them, namely, the third one, is a superimposition of the first H_2P reduction and the second C_{60} reduction. Moreover, the first and fourth waves are attributed to the first and third C_{60} reduction. The third wave can be justified by the second H_2P reduction (Supporting Information Figure S11). In general, the features of the ZnP analogues (i.e., **6a**,**b** and **7a**,**b**) resemble those discussed for the related H_2P derivatives. The only noticeable exception is the irreversibility of the reduction processes in both ZnP derivatives **6a**,**b** (Supporting Information Figures S13 and S14). A closer inspection of Table 1, which summarizes all the relevant potentials, infers the lack of significant electronic interactions between the redox- and photoactive moieties—H_2P, oligo-PPE, and C_{60} and ZnP, oligo-PPE, and C_{60}, respectively. In conclusion, both cyclic voltammetry and absorption measurements reveal the absence of electronic interactions between the different constituents. Nonetheless, the irreversibility of some of the investigated peaks is ascribed to the local conformational effects or to the adsorption phenomena at the electrode surfaces.

Quantum Chemical Investigation. Previous quantum chemical studies of oligo-PPE molecular wire systems led to the conclusion that rotations around the phenyl rings of these π-conjugated oligomers are not restricted due to very low rotational barriers (<2 kcal/mol).[22] However, the dihedrals between the phenyl rings tend to adopt nearly planar configurations in vacuo, which implies an improved π-conjugation throughout the entire oligo-PPE linker. Taking these findings into account, we have carefully looked at the rotational barrier between the phenyl rings in the monomer **9**[20] (see Figure 4 and 12), dimer **7a**, and trimer **7b**. The geometries of the zinc porphyrin (ZnP) and the free-base porphyrin (H_2P) derivatives were optimized at different levels of theory, namely, semiempirically (using the VAMP 10.0[23] program package with the AM1*[24] Hamiltonian) and by density functional theory (DFT) methods. The electronic ground states were optimized at the DFT level with the B3PW91[25] functional and a 6-31G(d) basis set as implemented in the Gaussian03[26] program package. To evaluate the rotational barriers, further single-point DFT calculations with improved basis sets including polarization and diffuse functions, i.e., 6-31+G(d,p) and 6-31++G(3df,2pd), were employed on structures with systematically varying dihedral

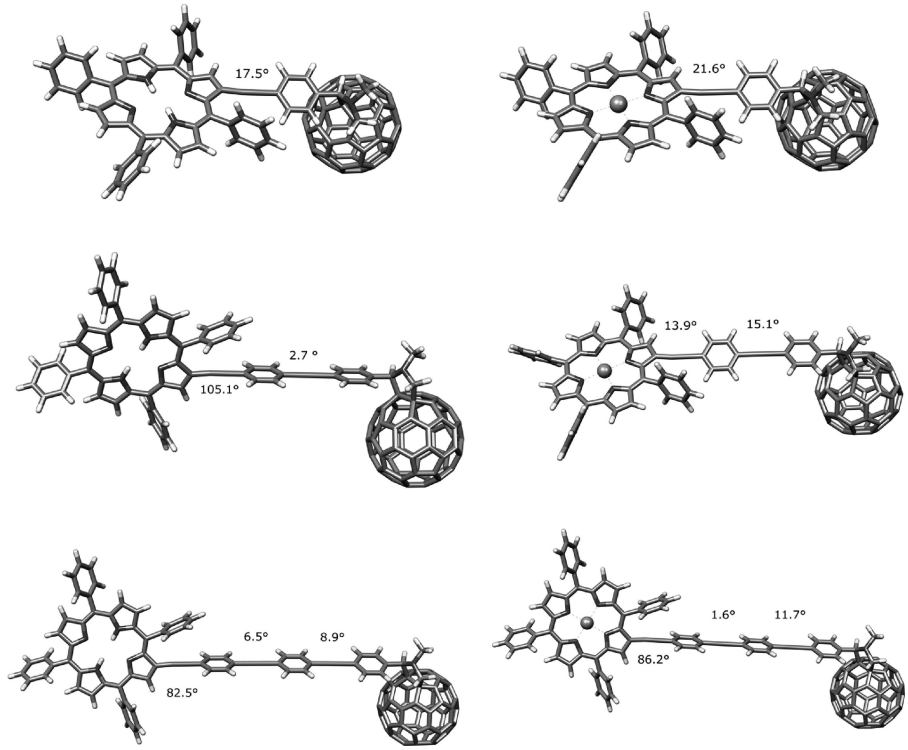

Figure 4. Optimized geometries (B3PW91/6-31G*) of the investigated triads **9**, **7a**, and **7b** including the dihedral angles between the phenyl rings and the bridge and the porphyrin moiety. Left column: free-base porphyrin derivatives. Right column: zinc porphyrin derivatives.

angles and compared to the optimized geometries. Interestingly, both monomeric derivatives of **9**, i.e., ZnP and H_2P, show a dihedral angle of approximately 20°, leading to close contacts between the porphyrins and the C_{60} cage (Figure 4). This explains the faster excited-state deactivation of the monomer[20] in comparison to the dimer and trimer.

These interactions allow a rapid through-space electron-transfer reaction, which was implied by photophysical measurements. The remaining oligomers contain nearly planar bridge configurations with dihedral angles in the range of ±14°, which is in a good agreement with our previous results.[22] As expected, the calculated barriers of rotation turned out to be lower than 1.4 kcal/mol, which proves the accuracy of the chosen DFT model according to other experimental and theoretical studies. These have shown that rotational barriers in oligo-PPE structures are between 0 and 0.96 kcal/mol.[27] Enthrallingly, in the trimer **7b** the angle between the adjacent phenyl ring and the porphyrin framework is roughly orthogonal, which might have a strong impact on the conjugation between the bridge and the porphyrins (Figure 4). Replacing the free base by the metallated porphyrin enhances this effect on account of increasing electron density stemming from the metal ion. Torsions around the ethynylene bond attached to the porphyrin apparently become more and more restricted with increasing length of the oligo-PPE linker which may impact the electron-transfer properties of these triads. Thus, a lack of coplanarity between the porphyrin and oligo-PPE, as can be evidenced in the trimer **7b**, might per se lead to a loss of electronic communication between donor and acceptor and is reflected in the longer charge-recombination rates.

In order to complement these findings, frontier orbitals schemes were analyzed. In particular, the highest occupied molecular orbitals/lowest unoccupied molecular orbitals (HOMO/LUMO) clearly reflect the donor−acceptor character of the systems. In line with our expectations, the HOMO and LUMO orbitals are strongly localized on the donor and the acceptor, i.e., the porphyrin and the fullerene, respectively (Figure 5). Significant overlap between the donor and the bridge suggests strong electronic coupling even in the ground state and facilitates electron injection from the excited porphyrin to the oligo-PPE connector. However, in the ZnP trimer coefficients of the HOMO are significantly present on the bridge structure and, hence, imply a stronger donor character of the ZnP derivatives in comparison to H_2P. Simultaneously, faster charge-separation dynamics, as evidenced throughout the photophysical study, confirm these findings. One possible explanation is that the linker of the ZnP derivative needs to accommodate higher electron density from the central metal ion. For that reason, electron density is redistributed into the adjacent vacant levels of the bridge. As a consequence, Coulomb repulsive interactions force the zinc porphyrin into an orthogonal arrangement to the phenyl units of the bridge. In the monomer, on the other hand, the short separation distance allows a facile transfer of electron density onto the LUMOs of the fullerene core. Noticeably, the electron-accepting features of the fullerene, as incorporated into the triads, are perfectly preserved. All oligomers exhibit a localization of the LUMO exclusively surrounding the symmetrical C_{60} cage. Furthermore, the short distance between donor and acceptor in the monomer **9** leads to significant overlap between HOMO and LUMO giving very fast electron-transfer processes. Important evidence for the interactions between the donor, bridge, and acceptor arises from an analysis of HOMO/LUMO orbital energies of the particular building blocks of the triads. Figure 6 relates the HOMOs and LUMOs of the building blocks to the corresponding orbitals in the triads. Herein, the significance of the matching of the orbital energy levels becomes apparent.

The most interesting subject of concern are the LUMO energies in the triads and C_{60}−oligo-PPE references, namely, 3.28 eV, which exactly matches the LUMO energy of the C_{60}−methyl fulleropyrolidine reference and clearly demonstrates the role of the C_{60} core as the predominant electron acceptor. Importantly, this feature is evident in all triads independently

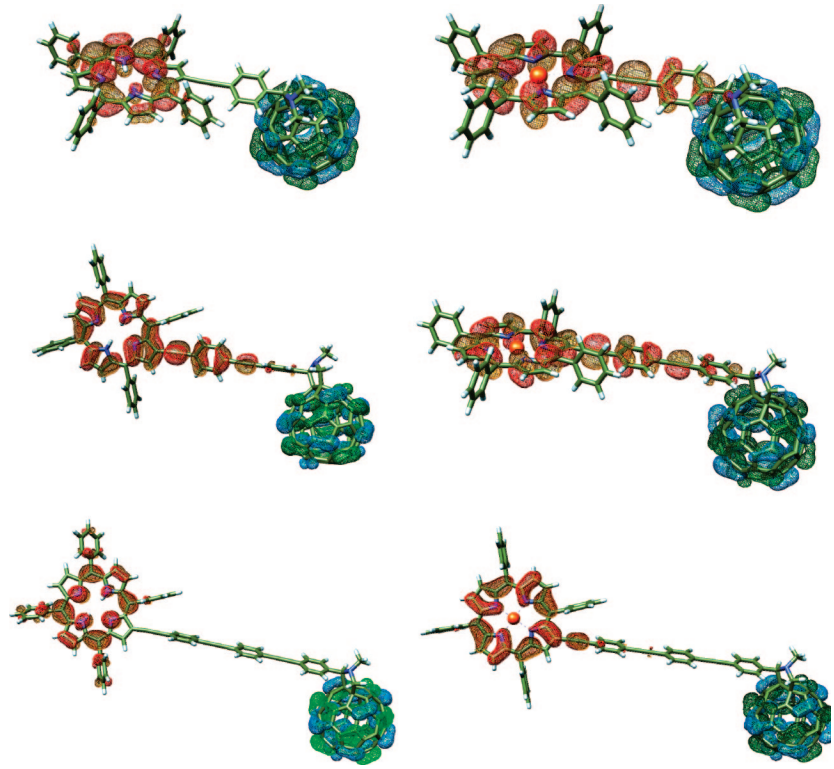

Figure 5. HOMO/LUMO orbital schemes as resulted from DFT optimizations (B3PW91/6-31G*) displaying the donor−acceptor character of the triads. The HOMOs are represented in orange-red and LUMOs in green-blue.

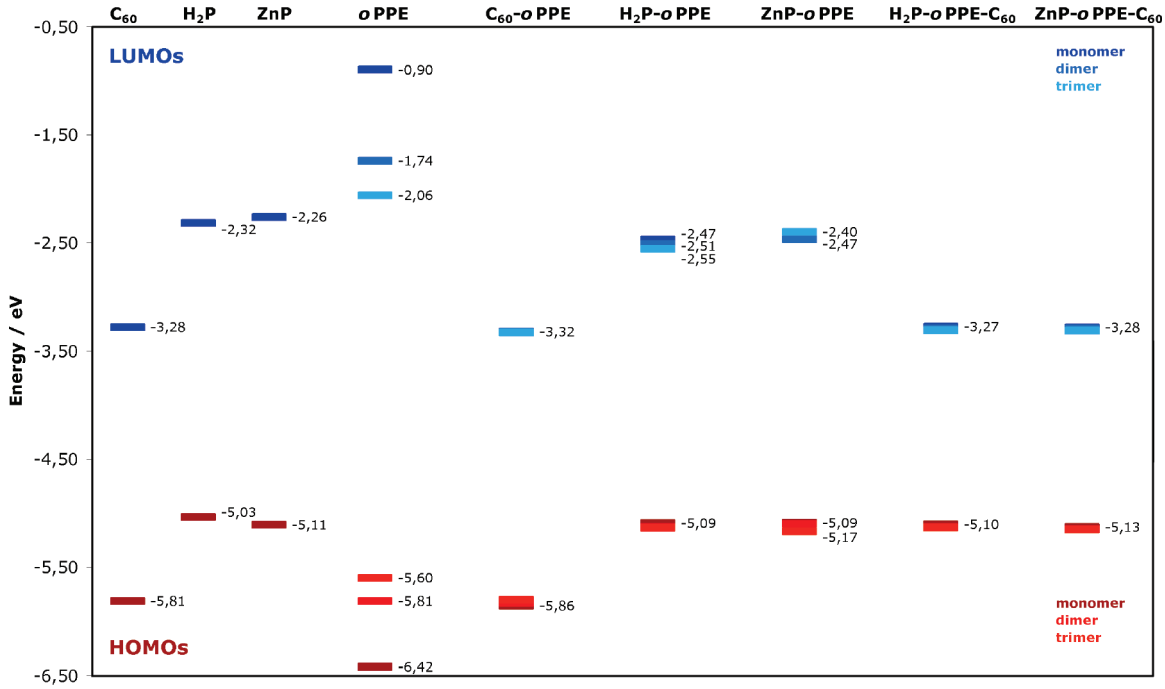

Figure 6. HOMO/LUMO orbital energies as resulted from DFT calculations (B3PW91/6-31++G(3df,3pd)) of the building blocks of the triads in relation to the triads. The HOMO energies are represented in red and LUMO energies in blue.

from the distance between donor and acceptor. On the other hand, a comparison of the HOMO energies of the triads and porphyrin−oligo-PPE conjugates to the HOMO energies of pristine H_2P and ZnP reveals the electron-donating features of the porphyrins. Here, the porphyrin HOMOs can be energetically compared to the corresponding HOMOs in the triads and the porphyrin−oligo-PPEs. Thus, attaching the oligo-PPE linker to the porphyrin derivatives does not alter the HOMO energy at all. Equally, the HOMO/LUMO energies of the donor and acceptor are preserved in all triads leading to the assumption that the electronic communication between both does not depend on the bridge length. Apparently, the bridge orbital energies do not mix with the energy levels of the donor and the acceptor which implies perfect conditions for a superexchange rather than a through-bond hopping mechanism for the electron-transfer processes. Nevertheless, the presence of significant overlap between the oligo-PPE linkers and the electron donor and acceptor, respectively, render the possibility of a thermally

induced hopping mechanism involving the bridge orbitals upon higher temperatures. Up the front, the energy difference of the orbitals of the oligo-PPE oligomers vanishes upon covalent binding to the porphyrins. Implicit extension of the π-system of the porphyrins onto the bridge is a possible explanation. On the other hand, in case of the fullerene, the HOMO and LUMO orbitals remain strongly localized on C_{60} implying a lack of electronic perturbation by the bridge. Moreover, the HOMO−LUMO gap of the oligo-PPE units is approximately 0.2 and 1.0 eV higher than in the corresponding porphyrin−oligo-PPE conjugates and the triads, respectively. This implies strong electronic coupling between the porphyrins and C_{60} which does not depend on the length of the oligo-PPE linker and leads to nearly distant-independent electron-transfer processes, as reflected by the extremely low β values of 0.11 Å^{-1}.

Furthermore, the HOMO/LUMO energies are in perfect agreement with the oxidation and reduction potentials obtained by the cyclic voltammetry study. Noteworthy, electrochemical measurements suggest that the reduction of the C_{60} moiety in **8a**,**b** does not depend on the oligo-PPE bridge and thus neglect considerable interactions between these two moieties. Our DFT calculations corroborate these features revealing that the reduction potentials of **8a**,**b** which appear around −3.8 eV comply with the LUMO energies of C_{60} (−3.3 eV). These values exceed the LUMO energies of oligo-PPE by more than 1.0 eV. Along with the assumption that the calculated orbital energies match the potentials obtained by electrochemistry, these findings imply a lack of electronic interactions between the redox-active moieties. For instance, the oxidation and reduction of **6a**,**b** are separated by an energy gap in the range of 2.2 and 2.3 eV which perfectly resembles the energy required for a HOMO to LUMO transition obtained in the calculations, namely, 2.6−2.7 eV.[28] Similarly, the potential gaps for the redox processes in the triads **7a**,**b** that appear between 1.6 and 1.9 eV are ascribed to the calculated HOMO to LUMO transitions at 1.8 eV.

Finally, local electron affinity mappings, as computed with Parasurf 07[29] and visualized using Tramp 1.1d,[30] corroborate the electron-transfer properties of **7a**,**b**. Previously studied oligo-PPE linkers between *ex*TTF (extended-tetrathiafulvalene) as electron donor and C_{60} as electron acceptor revealed an attenuation factor β of 0.21 Å^{-1}.[7e,f,22] The systems presented in this work exhibit lower attenuation factors, namely, a value of 0.11 Å^{-1}. In our foregoing studies the electron-transfer pathway of the linkers, i.e., the areas of high local electron affinity, was disrupted by the triple bonds due to their strong polarizing features. In addition, electron density minima appeared between the phenyl rings. Currently, the electron density in the porphyrin−oligo-PPE−C_{60} systems is more homogeneously distributed throughout the whole bridge due to the more electron-rich porphyrin donors in comparison to *ex*TTF. In line with the electron density, the local electron affinity exhibits a much more uniform distribution. Nevertheless, minima are localized at the triple-bond sites but the discrepancy between values of high (orange) and low (yellow to green) electron affinity is less pronounced due to higher electron density of these systems (Figure 7). These findings nicely comply with the lower β values obtained for the oligo-PPEs. Interestingly, the ZnP derivatives exhibit notably high electron affinity values at the central metal ion that reflect the inhomogeneous distribution of the electrons around the Zn atom facilitating electron injection into the bridge.

Photophysics. ***References.*** In steady-state experiments, all reference compounds (i.e., C_{60}, oligo-PPE, ZnP/H_2P) emit singlet excited-state energy in, however, different spectral regions of the solar spectrum. Although the fluorescence of oligo-PPE is typically observed in the 400−500 nm range, ZnP/H_2P emits in the 600−700 nm range and C_{60} emits with a maximum at 715 nm. The quantum yields vary substantially with values that range between 0.2 and 6 × 10^{-4} for the H_2P and C_{60} reference, respectively.

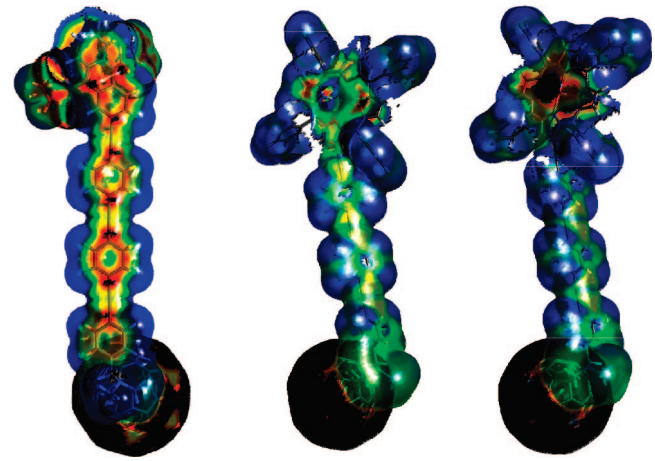

Figure 7. Local electron affinity maps of the *ex*TTF−oligo-PPE$_3$−C_{60} trimer compared to the porphyrin−oligo-PPE$_3$−C_{60}, **7b**, triads, scaling high to low in red to blue.

Also characteristic features were recorded in our ultrafast and fast transient absorption experiments. We see, for example, singlet excited states that are formed instantaneously: in case of the oligo-PPE singlet−singlet absorptions develop with maxima in the 500−700 nm range. Characteristics for ZnP/H_2P are 480 nm. For the C_{60} reference, on the other hand, the maximum is in the red at 880 nm. A fast intersystem crossing process (i.e., in the range of 10^8 s^{-1}) governs the fate of the metastable singlet excited states in all references (i.e., C_{60}, oligo-PPE, ZnP/H_2P). The corresponding formed triplet−triplet absorptions are all located in the range between 500 and 900 nm.

C_{60}−Oligo-PPE. Relative to the strong and long-lived emission of the oligo-PPE references, **4a**,**b**, the oligo-PPE emission in the C_{60}−oligo-PPE systems, **8a**,**b**, is nearly quantitatively quenched (Supporting Information Figure S7, top). Instead, a familiar fullerene fluorescence spectrum was found with a 0 → 0 emission at 715 nm, despite exclusive excitation of the oligo-PPE moiety (Supporting Information Figure S8, bottom). To reveal the mechanism of producing the emission, an excitation spectrum was taken. The excitation spectra of the **8a**,**b** references exactly matches the ground-state absorption of the oligo-PPE moieties. This implies a rapid transfer of singlet excited-state energy from the photoexcited oligo-PPE to the covalently linked fullerene.

Regarding the transient absorption measurements, immediately, after the laser excitation of **8a**,**b** at 387 nm, broadly absorbing transients with maxima between 400 and 500 nm (i.e., singlet−singlet absorptions of the oligo-PPE) were found (Supporting Information Figure S8). The spectral features recorded right after the laser pulse clearly confirmed—despite the presence of C_{60}—the successful formation of the oligo-PPE singlet excited state. However, the excited-state absorption was short-lived with lifetimes (i.e., <14 ps) that corroborated the efficient emission quenching.

Once the rapid disappearance of the excited oligo-PPE absorption comes to an end (i.e., ∼20 ps after the laser pulse), only characteristics of the fullerene singlet excited-state absorption remain. The noted maximum at 880 nm is reminiscent to that found for the reference C_{60}. In line with an energy transfer

TABLE 2: Selected Spectroscopic Date for the Investigated Triads 7a,b and the Appropriate Reference Compounds

	Φ_{fl}	τ_1 [ns]	k_{CS} [s^{-1}]	k_{CR} [s^{-1}]
C_{60} reference	6.0×10^{-4}	1.2		
H_2P reference	1.1×10^{-1}	9.8		
ZnP reference	4.0×10^{-2}	2.4		
7a	toluene: 6.1×10^{-2}	4.18	2.39×10^{8}	1.15×10^{6}
	THF: 4.4×10^{-2}			
	PhCN: 3.2×10^{-2}			
7b	toluene: 9.1×10^{-2}	5.97	1.68×10^{8}	0.84×10^{6}
	THF: 8.2×10^{-2}			
	PhCN: 7.9×10^{-2}			
Zn7a	toluene: 7.4×10^{-3}	0.45	2.22×10^{9}	1.44×10^{6}
	THF: 2.7×10^{-3}			
	PhCN: 2.1×10^{-3}			
Zn7b	toluene: 2.7×10^{-2}	1.18	0.85×10^{9}	1.10×10^{6}
	THF: 1.7×10^{-2}			
	PhCN: 1.3×10^{-2}			
8a	$<5.0 \times 10^{-4}$	1.4 ± 0.02		
8b	$<5.0 \times 10^{-4}$	1.4 ± 0.02		

mechanism the singlet−singlet absorption revealed a two-step grow-in dynamics. (Supporting Information Figure S9, top) The faster process stems from the direct excitation of the C_{60} core, while the slower component is ascribed to the actual transfer of excited-state energy. The latter assignment is based on the nearly identical dynamics (i.e., <18 ps) observed for the second component relative to those of the decays at 500 nm (time profiles at those wavelengths). Interestingly, the singlet−singlet excited-state deactivation in the dimer **8a** occurs on a faster time scale compared to the trimer **8b**. Yet, another process follows the conclusion of the energy transfer reaction in **8a**,**b**, whose outcome on the time scale of our femtosecond experiments is the formation of a distinct, new maximum at 700 nm (Supporting Information Figure S9, bottom). This absorption is in excellent agreement with the triplet excited-state absorption of the C_{60} reference, which infers that the underlying reaction involves intersystem crossing from the C_{60} singlet to the energetically lower-lying triplet manifold.

C_{60}−Oligo-PPE−ZnP/C_{60}−Oligo-PPE−H_2P. The aforementioned energy transfer is in all C_{60}−oligo-PPE (**8a** and **b**) nearly quantitative and helps to concentrate the singlet excited-state energy at the fullerene end. Notable, the contribution from an exothermic electron transfer is inappreciably small. This general pattern is not affected when linking ZnP/H_2P to the other end of the wire, C_{60}−oligo-PPE−ZnP/C_{60}−oligo-PPE−H_2P. In case of exciting the oligo-PPE part in C_{60}−oligo-PPE−ZnP/C_{60}−oligo-PPE−H_2P (i.e., 300−500 nm range), a rapid intramolecular transduction of energy—as evidenced by fluorescence quantum yields of $<5.0 \times 10^{-4}$ (see Supporting Information Figure S7)—funnels the excited-state energy to the C_{60} core, generating ^{1}*C_{60} with nearly unity quantum yields (Table 2). Drawing the attention to the porphyrin emission, please note that in contrast to previously studied C_{60}−oligo-PPE−donor systems, ZnP and H_2P not only absorb notably in the current C_{60}−oligo-PPE−donor systems, but their strong fluorescence dominates large parts of the spectrum. Interestingly, the ZnP/H_2P centered fluorescence is appreciably quenched in all C_{60}−oligo-PPE−ZnP/C_{60}−oligo-PPE−H_2P—regardless of the excitation wavelength (i.e., Soret- or Q-band region)—prompting to the fact that C_{60} must enhance the fluorescence deactivation (vide infra). Figure 8 illustrates the fluorescence quenching of the ZnP and H_2P oligomers in tetrahydrofuran (THF).

To shed light on the nature of the product, evolving from this intramolecular deactivation, complementary time-resolved fluorescence and transient absorption measurements were necessary. Let us first direct our attention to the fluorescence lifetime measurements. A notable shortening of the ZnP/H_2P fluorescence lifetimes are seen in C_{60}−oligo-PPE−ZnP/C_{60}−oligo-PPE−H_2P (Table 2). Upon modifying the solvent polarity from toluene ($\varepsilon = 2.4$) over THF ($\varepsilon = 7.6$) to benzonitrile ($\varepsilon = 24.8$) a gradual intensification of the quenching is discernible, as evidenced by the decreasing quantum yields in Table 2. We hypothesize that the underlying solvent dependence is due to an intramolecular electron transfer between the photoexcited ZnP/H_2P donors and C_{60} to yield $C_{60}^{\bullet-}$−oligo-PPE−$ZnP^{\bullet+}$/$C_{60}^{\bullet-}$−oligo-PPE−$H_2P^{\bullet+}$.

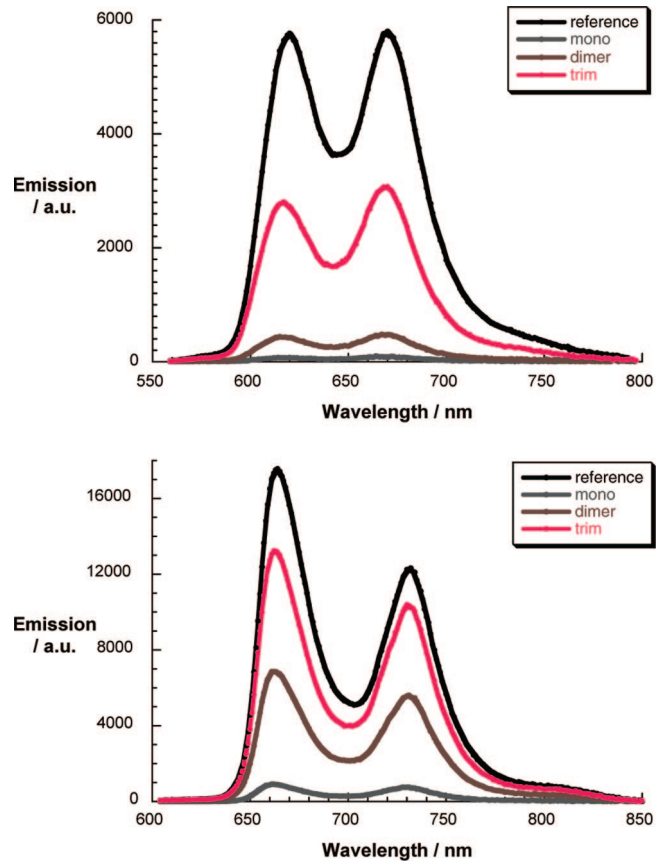

Figure 8. Fluorescence spectra of C_{60}−oligo-PPE−ZnP and ZnP (upper part) and C_{60}−oligo-PPE−H_2P and H_2P (lower part) in THF upon 440 and 460 nm excitation, respectively, with solutions displaying the same optical density at the excitation wavelengths (i.e., 0.1).

In transient absorption measurements, we focused exclusively on the generation of the singlet excited states of ZnP/H_2P. The overlapping absorptions of all components renders any other analysis ambiguous, though we must assume that in accordance with previous work that starting with the C_{60} singlet excited state a similar reaction pattern will evolve. Instead of seeing, however, the slow intersystem crossing dynamics, as the ZnP/H_2P references, the singlet−singlet absorption decays in the presence of C_{60} acceptors with accelerated dynamics. An important aspect is that the singlet excited-state lifetimes match quantitatively those values derived in the fluorescence experiments. Spectroscopically, the transient absorption changes, taken after the completion of the decay, bear no resemblance with any triplet excited state (vide infra). Again, varying the solvent polarity from THF to benzonitrile leads to an acceleration of the singlet deactivation. This supports our earlier hypothesis that an intramolecular electron transfer, yielding $C_{60}^{\bullet-}$−oligo-PPE−$ZnP^{\bullet+}$/$C_{60}^{\bullet-}$−oligo-PPE−$H_2P^{\bullet+}$, governs the ZnP/H_2P singlet excited-state deactivation.

Spectroscopic evidence for the radical pair formation was lent from the features developing in parallel with the disappearance

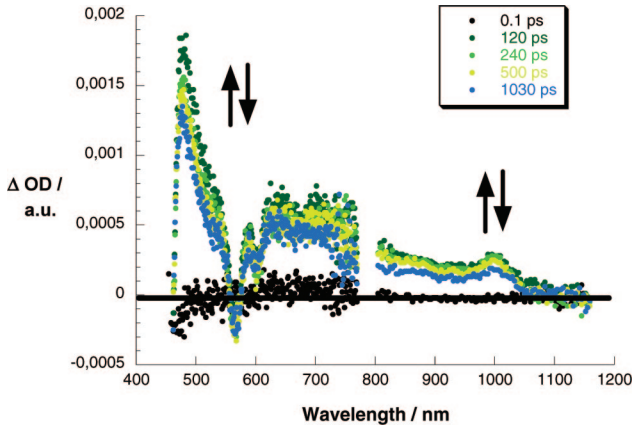

Figure 9. Differential absorption spectra (visible and near-infrared) obtained upon femtosecond flash photolysis (387 nm, 200 nJ) of C_{60}−oligo-PPE_2−ZnP in argon-saturated THF with several time delays between 0 and 1000 ps at room temperature, illustrating the charge transfer.

of the ZnP/H_2P singlet−singlet absorption. In the visible region, the observed maxima between 600 and 700 nm as well as 480 nm correspond to the one-electron-oxidized π-radical cations of ZnP ($ZnP^{\bullet+}$) and H_2P ($H_2P^{\bullet+}$), respectively, whereas in the near-infrared region the 1000 nm maximum resembles the signature of the one-electron-reduced form of C_{60} ($C_{60}^{\bullet-}$)—Figure 9.

Since no charge-transfer was evidenced in the C_{60}−oligo-PPE references, we exclude the involvement of a transient oxidized oligomer, $C_{60}^{\bullet-}$−oligo-$PPE^{\bullet+}$−ZnP/$C_{60}^{\bullet-}$−oligo-$PPE^{\bullet+}$−H_2P throughout the charge-separation reaction. Hence, we imply that in the dimer- and trimer-based systems charge separation occurs within a single step. Figure 10 compares the charge-transfer dynamics of the dimer- to the trimer-based ZnP system.

To examine the charge-recombination dynamics the spectral fingerprints of the C_{60} π-radical anion and that of the ZnP/H_2P π-radical cations are useful probes. Both spectral attributes are persistent on the picosecond time scale and only start to decay slowly in the nanosecond regime. Time absorption profiles illustrate that $C_{60}^{\bullet-}$−oligo-PPE−$ZnP^{\bullet+}$/$C_{60}^{\bullet-}$−oligo-PPE−$H_2P^{\bullet+}$ decay via a single step. The charge-recombination dynamics within these systems were determined accurately by fitting the decays of both fingerprints to a monoexponential rate law in complementary nanosecond experiments.

Importantly, comparing solvents of different polarity, namely, THF and benzonitrile, stabilizing effects for all $C_{60}^{\bullet-}$−oligo-PPE−$ZnP^{\bullet+}$/$C_{60}^{\bullet-}$−oligo-PPE−$H_2P^{\bullet+}$ radical pairs were seen toward the more polar solvents. This trend prompts to charge-recombination dynamics that are in the normal region of the Marcus parabola. For that reason, we have calculated the driving forces for charge separation and charge recombination in each of the three solvents according to the method by Weller.[31] Supporting Information Table S1 represents the calculated ΔG values for the charge separation and recombination placing the back electron transfer onto the normal regime of the Marcus parabolas. On the basis of these values it was possible to illustrate the different possible reaction pathways in a state diagram (Figure 11).

Plotting the electron-transfer behavior—both charge-separation rate and charge-recombination rate—as a function of donor−acceptor separation including the results from the previously published "monomer"[20] (Figure 12) led to linear dependences for THF and benzonitrile as solvents. From fluorescence lifetime

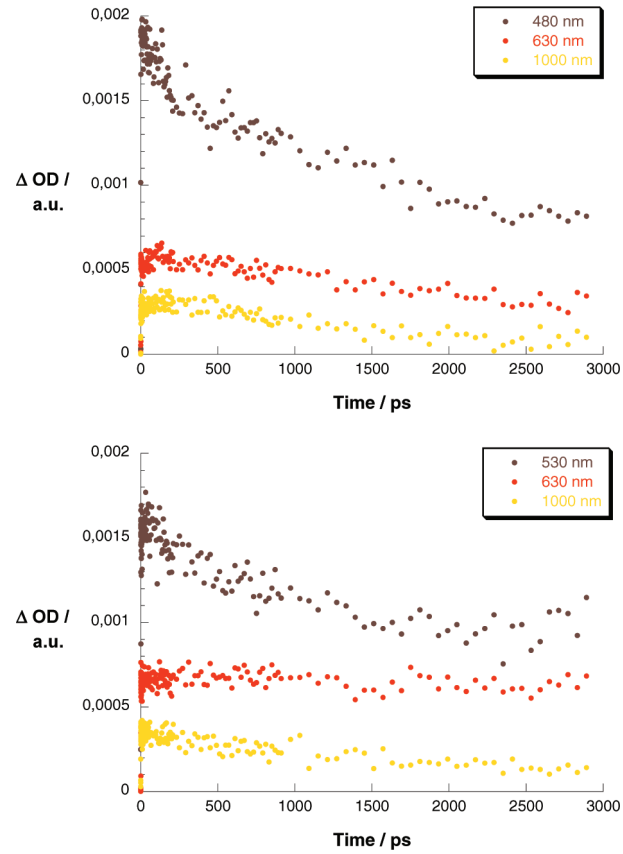

Figure 10. Upper part: time−absorption profiles at 480, 640, and 1000 nm of the differential absorption measurements with C_{60}−oligo-PPE_2−ZnP in THF solutions. Lower part: time−absorption profiles at 530, 630, and 1000 nm of the differential absorption measurements with C_{60}−oligo-PPE_3−ZnP in THF solutions—monitoring the charge-transfer processes.

and transient absorption kinetic measurements (femto- and nanosecond time scales) we determine attenuation factors (β) for our ensembles as 0.11 $Å^{-1}$, which are exceptionally small (Figure 13).

Conclusion

A series of novel porphyrin−wire−fullerene systems in which the wire component is covalently bound to the β-pyrrole carbon atom of the porphyrin macrocycle has been synthesized and characterized. Upon photoexcitation both free-base and related zinc derivatives systems are capable of electron-transfer reactions from the electron-donating porphyrin to the electron-accepting C_{60} moiety in polar solvent environment (i.e., THF). Long-lived charge-separated states with lifetimes in the order of hundred of nanoseconds have been demonstrated. Furthermore, the lifetimes of the radical ion pair tend to increase with increasing distance between the two photoactive units. Since the charge-separation reaction occurs over a long distance, namely, up to 23 Å, when $n = 3$, a through-bond mechanism, where the bridge plays an important role, is plausible; in addition to that, transient absorption and cyclic voltammetry studies did not reveal accessible oxidized states of the linker. Therefore, electron transfer via a superexchange mechanism seems to be the most probable operative mode. The studied systems ($n = 2, 3$) indicate a linear distance dependence of the electron-transfer rate constant—considering the edge-to-edge distance between the two photoactive chromophores—with an attenuation factor β equal to 0.11 $Å^{-1}$. This value complements those

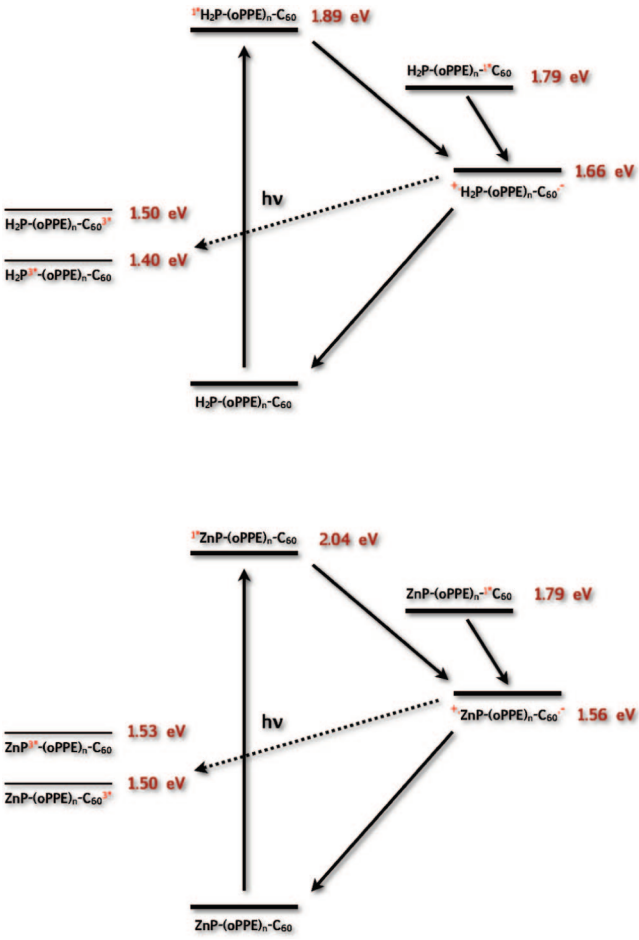

Figure 11. Schematic illustration of the reaction pathways in photexcited C_{60}−oligo-PPE_2−H_2P (top) and C_{60}−oligo-PPE_2−ZnP (bottom) with the state energies as determined in THF. The different deactivation pathways are indicated by arrows.

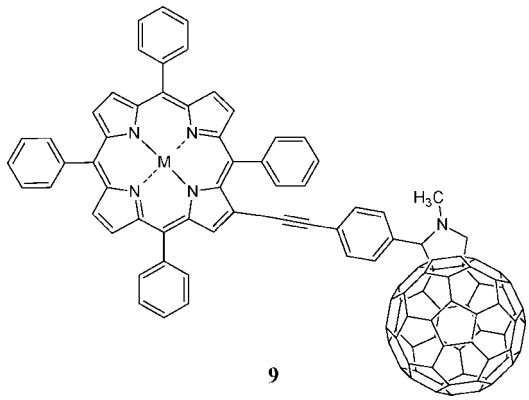

9

Figure 12. Porphyrin−fullerene system with one ethynylenephenylene subunit (n = 1). M = 2H, Zn.

reported in previous studies,[5] taking the damping factor β of 0.21 Å^{-1} into account, which was found in similar systems bearing *ex*TTF[7e] as donor moiety. Thus, at this point, we would like to underline the dependence of the wirelike behavior of the linker on the donor features.

From UV−vis absorption and cyclic voltammetry studies we can exclude a complete extension of the porphyrin HOMO along the whole length of the linker for compounds **7a**,**b** and **6a**,**b** for two reasons: (1) no red shift of the Soret band of the porphyrin upon an increase of the linker length is observed in the UV−vis spectra, which has been previously observed for

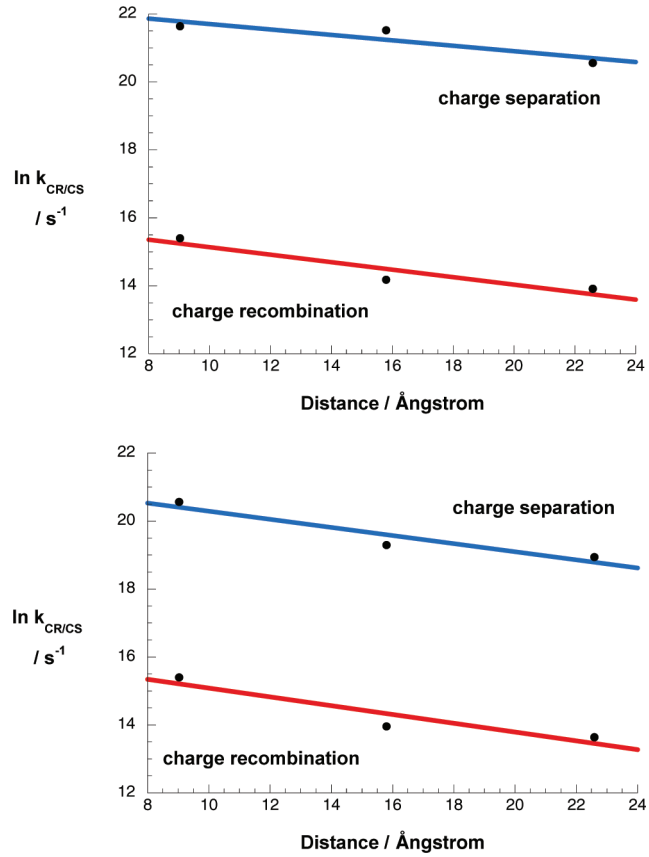

Figure 13. Edge-to-edge distances (R_{EE}) dependence of charge-separation (ln k_{CS}) and charge-recombination (ln k_{CR}) rate constants of H_2P−oligo-PPE_n−C_{60} (upper part) and ZnP−oligo-PPE_n−C_{60}) (lower part) triads (n = 1, 2, 3) in nitrogen-saturated THF at room temperature. The slope represents β with the value of 0.11 Å^{-1}.

the oligo-vinylenephenylene β-substituted porphyrin,[32] (2) the oxidation potential of the porphyrin macrocycle is nearly unaffected by the length of the linker during cyclic voltammetry. These findings imply that the conformation of the porphyrin relative to the phenyl rings of the bridge prevents the full conjugation between donor and the linker. On the other hand, the oligo-ethynylenephenylenes demonstrate a rather effective wirelike behavior resulting from a possible coplanarity of the phenyl rings.[5]

Quantum chemical investigations provided further understanding for the influence of electronic and structural properties of the investigated triads **7a**,**b** and **6a**,**b** on their charge-transfer features. Geometry optimizations suggest a nearly planar bridge configuration of the oligo-PPEs, which supports the extended π-conjugation of these systems. Differences between the H_2P and ZnP derivatives have been found regarding the dihedral angle between the porphyrins and the bridge, which might lead to a loss of electronic communication between donor and acceptor in **7** and reflects the longer charge-recombination rates. Further analysis of the electronic structure revealed a strong localization of the HOMOs and LUMOs on the electron-donating porphyrin and electron-accepting fullerene, respectively, proposing an increased donor character of the Zn derivatives. Regardless of the incorporation of C_{60} into the triads, its electron-accepting features turned out to be perfectly preserved. Furthermore, the matching of the HOMO/LUMO energy levels of the single components of the triads plays a major role for efficient electronic communication between donor and acceptor, which was also proved by the electrochemical investigation. Thus, the mechanism of the charge-transfer

processes seems to remarkably depend on the structural properties of the linker between donor and acceptor and its conjugation into the porphyrin/C_{60} moieties. These findings have been corroborated by local electron affinity mappings.

Experimental Section

General Methods. ^{1}H NMR spectra were recorded as $CDCl_3$ solutions on a Bruker AM-300 instrument using residual solvent signal as an internal standard. Chemical shifts are given as δ values. Fast atom bombardment (FAB) mass spectra were measured on a VG-4 spectrometer using *m*-nitrobenzyl alcohol (NBA) as a matrix. Gas chromatography (GC) mass spectra were recorded on a VG-4 spectrometer equipped with a 30 mt Supelco SPB-5 capillary column. MALDI mass spectra were performed with a MALDI-TOF Reflex IV (Bruker-Daltonics) in reflector mode, using a 337 nm nitrogen laser (8 Hz). A 2 mg/mL 2,5-dihydroxybenzoic acid (gentysic acid) solution in CH_3CN/TFA (0.1% solution) was used as a matrix. UV−vis spectra were recorded on a Varian Cary 50 Scan spectrophotometer in toluene solution. Steady-state fluorescence studies were carried out on a Fluoromax 3 (Horiba) instrument, and all the spectra were corrected for the instrument response. Time-resolved fluorescence spectra were recorded on a Photon Technology International Company lifetime spectrofluorometer in the nanosecond time domain, with a 337 nm nitrogen laser and elaborated with Felix software. The femtosecond transient absorption studies were performed with 387 nm laser pulses (1 kHz 150 fs pulse width) from an amplified Ti:Sapphire laser system (model CPA 2101, Clark-MXR Inc.). Nanosecond laser flash photolysis experiments were performed with 532 nm laser pulses from a Quanta-Ray CDR Nd:YAG system (6 ns pulse width) in a front face geometry. Cyclic voltammetry was carried out with a Autolab electrochemical system, Eco Chemie equipped with PG Stat-12. Current−voltage curves were recorded using GPES, Eco Chemie software. A three-electrode system was used and consisted of a platinum button working electrode, a platinum wire counter electrode, and an SCE reference electrode. This reference electrode was separated from the bulk of the solution by a fritted-glass bridge filled with solvent/supporting electrolyte mixture. All potentials are referenced to the SCE.

Chemicals. Silica gel 60 (70−230 and 230−400 mesh, Merck) was used for column chromatography. 1,2-Dichlorobenzene (DCB) for electrochemistry was purchased from Aldrich Chemical Co. and purified by several washings with concd H_2SO_4 and distilled over P_2O_5 under vacuum prior to use. Tetra-*n*-butylammonium hexafluorophosphate from Aldrich Chemical Co. was recrystallized from ethyl acetate and dried under vacuum at 40 °C for at least 1 week prior to use. High-purity-grade nitrogen gas was purchased from Rivoira. C_{60} was purchased from Term-USA. All other reagents and solvents were from Fluka Chem. Co., Aldrich Chem. Co., or Carlo Erba and were used as received. 4-Ethynylbenzaldehyde[18] and 2-bromo-5,10,15,20-tetraphenylporphyrin[20] were synthesized following the procedures reported in the literature.

1-Iodo-4-(trimethylsilyl)ethynyl-benzene (2). 1,4-Diiodobenzene (7.6 g, 23 mmol), $PdCl_2(PPh_3)_2$ (212 mg, 3×10^{-4} mol), and CuI (115 mg, 6×10^{-4} mol) were dissolved in dry THF (50 mL), then dry triethylamine (KOH, 3 mL) was added. The solution was left under nitrogen atmosphere at 40 °C, and a THF solution (10 mL) of trimethylsilylacetylene (1.40 g, 14 mmol) was added dropwise over 1 h. After 6 h, the reaction was stopped and solvent evaporated under vacuum The residue was chromatographed on silica gel column eluting with petroleum ether (40−70°). The desired product was obtained as white needles in a 62% yield. MS (GC): *m*/*z* 300 [M^+], 285 [$M-15]^+$, 158 [$285-127]^+$. ^{1}H NMR (300 MHz, $CDCl_3$,): δ (ppm) 7.66 (d, $^3J = 8.8$ Hz, 2H), 7.20 (d, $^3J = 8.8$ Hz, 2H), 0.26 (s, 9H).

General Procedure for the Sonogashira Coupling in the Synthesis of the Oligo-Phenyleneethynylenes. 1-Iodo-4-(trimethylsilyl)ethynyl-benzene and the appropriate aldehyde derivative were dissolved in a 1:1 molar ratio in 60 mL of dry THF (distilled over $LiAlH_4$); 3 mL of dry triethylamine (KOH) was added with 0.03 equiv of $PdCl_2(PPh_3)_2$ and 0.07 equiv of CuI. The mixture was left to react under a nitrogen atmosphere at 40 °C for 6 h, then the solvent was removed under vacuum, and the crude product was purified over silica gel column chromatography eluting with CH_2Cl_2/petroleum ether (40−70°), 30:70.

4-[4′-(Trimethylsilyl)ethynyl]phenyl-ethynylbenzaldehyde, (TMS−Oligo−PPE$_2$−CHO) (4a). Starting reagents: 1-iodo-4-(trimethylsilyl)ethynyl-benzene (700 mg, 2.3 mmol) and 4-ethynylbenzaldehyde (305 mg, 2.3 mmol). Yield 65% (450 mg). MS (GC): *m*/*z* 302 [M^+]. ^{1}H NMR (300 MHz, $CDCl_3$,): δ (ppm) 10.05 (s, 1H), 7.89 (d, $^3J = 8.3$ Hz, 2H), 7.69 (d, $^3J = 7.5$ Hz, 2H), 7.51 (m, 4H), 0.28 (s, 9H). UV−vis (toluene): λ_{max} (nm) (ε) = 325 (31 300), 347 (28 200 mol^{-1} dm^3 cm^{-1}).

4-{4′-[4″-(Trimethylsilyl)ethynylphenyl]ethynylphenyl}-ethynylbenzaldehyde, (TMS−Oligo-PPE$_3$−CHO) (4b). Starting reagents: 4-[(4′-ethynyl)phenyl]-ethynylbenzaldehyde (157 mg, 6.8×10^{-4} mol), 1-iodo-4-(trimethylsilyl)ethynyl-benzene (205 mg, 6.8×10^{-4} mol). The desired product was recrystallized from $CHCl_3$/petroleum ether (40−70°), affording 170 mg of pale yellow-white needles, yield 65%. MS (FAB): *m*/*z* 402 [M^+]. ^{1}H NMR (300 MHz, $CDCl_3$,): δ (ppm) 10.05 (s, 1H), 7.90 (d, $^3J = 7.98$ Hz, 2H), 7.70 (d, $^3J = 7.98$ Hz, 2H), 7.55 (s, 4H), 7.48 (s, 4H), 0.28 (s, 9H). UV−vis (toluene): λ_{max} (nm) (ε) = 345 (65 800 mol^{-1} dm^3 cm^{-1}).

General Procedure for the Terminal Triple-Bond Deprotection Reaction. Oligomers having terminal-protected triple bond were dissolved in 50 mL of $CHCl_3$, and then a K_2CO_3-saturated methanol solution (10 mL) was added dropwise under nitrogen atmosphere. After 2 h, water (50 mL) was added to the organic solution. The organic phase was separated, and the aqueous phase was twice extracted with 25 mL of chloroform. The combined organic solutions were dried over anhydrous Na_2SO_4, filtered, and the solvent was evaporated under vacuum.

4-[(4′-Ethynyl)phenyl]-ethynylbenzaldeide (5a). The reaction is almost quantitative. ^{1}H NMR (300 MHz, $CDCl_3$,): δ (ppm) 10.05 (s, 1H), 7.90 (d, $^3J = 7.8$ Hz, 2H), 7.70 (d, $^3J = 7.8$ Hz, 2H), 7.52 (s, 4H), 3.22 (s, 1H).

4-{4′-[4″-(Ethynyl)phenyl]ethynylphenyl}-ethynylbenzaldehyde (5b). The reaction is almost quantitative.^{1}H NMR (300 MHz, $CDCl_3$,): δ (ppm) 10.05 (s, 1H), 7.90 (d, $^3J = 7.98$ Hz, 2H), 7.70 (d, $^3J = 7.98$ Hz, 2H), 7.55 (s, 4H), 7.50 (s, 4H), 3.20 (s, 1H).

General Procedure for the Sonogashira Coupling in the Synthesis of Porphyrin−Oligo−PPE Systems. A three-neck round-bottom flask, fitted with a condenser, was carefully deoxygenated with a strong stream of dry argon; after that a solution of 2-bromo-5,10,15,20-tetraphenylporphyrin (1 equiv) and the appropriate aldehyde oligomer (1.5 equiv) in toluene/triethylamine, 5:1 (60 mL), was added. The solution was deaerated for 30 min with argon bubbling, and then $Pd(dba)_2$ (0.2 equiv) and $AsPh_3$ (1.5) were added. The solution was deaerated for further 5 min; after that the argon inlet was placed 1 cm above the solution. The argon flow rate was turned up slightly and the reaction was left under nitrogen at 60 °C. After

16 h, the mixture was cooled at room temperature and the solvent was evaporated. The crude product was dissolved in dichloromethane and washed several times with water. The organic solution was dried over anhydrous Na_2SO_4, and the solvent was evaporated under vacuum. The desired product was purified by silica gel column chromatography.

H_2P−Oligo−PPE_2−CHO (6a). The crude product was purified by column chromatography on silica gel eluting with $CHCl_3$/petroleum ether (40−70°), 1:1. The first compound eluted from the column was $AsPh_3$; after that the polarity of eluting mixture was gradually increased up to $CHCl_3$/petroleum ether (40−70°), 70:30. The desired porphyrin obtained from the column was recrystallized from dichloromethane/methanol to give a purple powder (yield 65%). MS (FAB): *m*/*z* 842 [M^+]. ^{1}H NMR (300 MHz, $CDCl_3$): δ (ppm) 10.06 (s, 1H), 9.10 (s, 1H), 8.90 (s, 2H), 8.85 (d, ^3J = 5.9 Hz, 1H), 8.79 (s, 2H), 8.77 (d, ^3J = 5.9 Hz, 1H), 8.23 (br m, 5H), 7.91 (d, ^3J = 7.8 Hz, 2H), 7.80−7.66 (br m, 17H), 7.54 (d, ^3J = 7.8 Hz, 2H), 7.38 (d, 2H; J = 7.8), −2.65 (s, 2H). UV−vis (toluene): λ_{max} (nm) (ε) = 333 (28 900), 378 (30 600), 430 (194 000), 524 (20 000), 560 (6900), 603 (5400), 659 (3500 mol^{-1} dm^3 cm^{-1}).

H_2P−Oligo−PPE_3−CHO (6b). The crude product was purified by column chromatography on silica gel eluting with $CHCl_3$/petroleum ether (40−70°), 1:1. The first compound eluted from the column was $AsPh_3$ after that the polarity of eluting mixture was gradually increased up to $CHCl_3$/petroleum ether (40−70°), 3:2. The desired porphyrin obtained from the column was recrystallized from dichloromethane/methanol to give a purple powder (yield 70%). MS (FAB): *m*/*z* 942 [M^+]. ^{1}H NMR (300 MHz, $CDCl_3$): δ (ppm) 10.04 (s, 1H), 9.10 (s, 1H), 8.90 (s, 2H), 8.85 (d, ^3J = 4.5 Hz, 1H), 8.79 (s, 2H), 8.77 (br d, ^3J = 5.2 Hz, 1H), 8.23 (br m, 5H), 7.91 (d, ^3J = 8.3 Hz, 2H), 7.80−7.66 (br m, 15H), 7.70 (d, ^3J = 8.3 Hz, 2H), 7.58 (s, 4H), 7.53 (d, ^3J = 8.3 Hz, 2H), 7.38 (d, ^3J = 8.3 Hz, 2H), −2.67 (s, 2H). UV−vis (toluene): λ_{max} (nm) (ε) = 344 (57 000), 373 (54 000), 430 (239 000), 524 (24 600), 560 (9300), 603 (6700), 659 (4400 mol^{-1} dm^3 cm^{-1}).

General Procedure for the Synthesis of Porphyrin−Oligo-PPE−Fullerene and Oligo-PPE−Fullerene Systems. A mixture of appropriate aldehyde compound (1 equiv), C_{60} (1.5 equiv), and *N*-methylglicine (10 equiv with respect to C_{60}) was refluxed for 24 h in anhydrous toluene (distilled from Na) under nitrogen atmosphere. After cooling, the solvent was evaporated and the residue was directly purified on silica gel column, recovering the unreacted [60]fullerene as first fraction, the desired reaction product as second one, and the unreacted porphyrin as the third one.

H_2P−Oligo-PPE_2−C_{60} (7a). Eluant mixture: toluene/petroleum ether (40−70°), 70:30. The product was recovered as black-purple powder (yield 57%). MS (MALDI): *m*/*z* 1590 [M + H]$^+$, 869 [M − 720]$^+$, 720 [M − 869]$^+$. ^{1}H NMR (300 MHz, $CDCl_3$): δ (ppm) 9.09 (s, 1H), 8.89 (s, 2H), 8.83 (d, ^3J = 5.8 Hz, 1H), 8.77 (s, 2H), 8.75 (d, ^3J = 5.8 Hz, 1H), 8.21 (br m, 5H), 7.80−7.66 (br m, 19H), 7.48 (d, ^3J = 7.8 Hz, 2H), 7.34 (d, ^3J = 7.8 Hz, 2H), 4.92 (d, ^2J = 9.8 Hz, 1H), 4.84 (s, 1H), 4.16 (d, ^2J = 9.8 Hz, 1H), 2.80 (s, 3H), −2.67 (s, 2H). UV−vis (toluene): λ_{max} (nm) (ε) = 323 (66 700), 430 (215 000), 524 (22 300), 560 (8100), 603 (6200), 659 (3800 mol^{-1} dm^3 cm^{-1}).

H_2P−Oligo-PPE_3−C_{60} (7b). Eluant mixture: toluene/petroleum ether (40−70°), 70:30. The product was recovered as black powder (yield 52%). MS (MALDI): *m*/*z* 1690 [M + H]$^+$, 969 [M − 720]$^+$, 720 [M − 969]$^+$. ^{1}H NMR (300 MHz, $CDCl_3$): δ (ppm) 9.10 (s, 1H), 8.89 (s, 2H), 8.85 (d, ^3J = 5.3 Hz, 1H), 8.78 (s, 2H), 8.75 (d, ^3J = 5.3 Hz, 1H), 8.23 (br m, 5H), 7.80−7.50 (br m, several signals difficult to resolve and integrate), 7.48 (d, ^3J = 7.8 Hz, 2H), 7.34 (d, ^3J = 8.3 Hz, 2H), 4.90 (d, ^2J = 9.8 Hz, 1H), 4.79 (s, 1H), 4.13 (d, ^2J = 9.8 Hz, 1H), 2.78 (s, 3H), −2.67 (s, 2H). UV−vis (toluene): λ_{max} (nm) (ε) = 334 (90 900), 430 (239 000), 524 (25 000), 560 (9400), 603 (6900), 659 (4300 mol^{-1} dm^3 cm^{-1}).

TMS−Oligo-PPE_2−C_{60} (8a). Starting reagents: C_{60} (55 mg, 7.6 × 10^{-5} mol), 4-[4′-(trimethylsilyl)ethynyl]phenyl-ethynyl-benzaldeide (16 mg, 5.2 × 10^{-5} mol) and *N*-methylglicine (70 mg, 7.6 × 10^{-4} mol). Eluant mixture: petroleum ether (40−70°)/toluene, 3:2. Obtained 33 mg of brown powder as final product (yield 60%). MS (MALDI): *m*/*z* 1049 [M^+], 720 [M − 329]$^+$. ^{1}H NMR (300 MHz, $CDCl_3$): δ (ppm) 7.82 (br d, 2H), 7.61 (d, ^3J = 7.6 Hz, 2H), 7.45 (s, 4H), 5.02 (d, ^2J = 9.8 Hz, 1H), 4.98 (s, 1H), 4.29 (d, ^2J = 9.8 Hz, 1H), 2.84 (s, 3H), 0.26 (s, 9H). UV−vis (toluene): λ_{max} (nm) (ε) = 312 (63 800), 332 (64 900 mol^{-1} dm^3 cm^{-1}).

TMS−Oligo-PPE_3−C_{60} (8b). Starting reagent: TMS−oligo-PPE_3−CHO (20 mg, 5 × 10^{-5} mol), C_{60} (54 mg, 7.5 × 10^{-5} mol), and *N*-methylglicine (67 mg, 7.5 × 10^{-4} mol). Eluant mixture: petroleum ether (40−70°)/toluene, 3:2. Obtained 40 mg of brown-reddish powder as final product (yield 70%). MS (MALDI): *m*/*z* 1149 [M^+], 720 [M − 429]$^+$. ^{1}H NMR (300 MHz, $CDCl_3$): δ (ppm) 7.85 (br d, 2H), 7.63 (d, ^3J = 8.3 Hz, 2H), 7.50 (s, 4H), 7.46 (s, 4H) 5.02 (d, ^2J = 9.1 Hz, 1H), 4.98 (s, 1H), 4.29 (d, ^2J = 9.1 Hz, 1H), 2.84 (s, 3H), 0.27 (s, 9H). UV−vis (toluene): λ_{max} (nm) (ε) = 336 (90 500), 362 (54 200 sh, mol^{-1} dm^3 cm^{-1}).

General Procedure for Zinc Insertion. To a solution of starting compound (porphyrins or dyad) in chloroform a saturated solution of $Zn(AcO)_2$ in methanol was added, and the mixture was left to react at room temperature under nitrogen for 2 h. The solvent was evaporated, and the product was purified using a plug of silica gel, eluting with chloroform.

ZnP−Oligo-PPE_2−CHO (Zn6a). Yield: 97%. MS (MALDI): *m*/*z* 905 [M^+]. ^{1}H NMR (300 MHz, $CDCl_3$): δ (ppm) 10.04 (s, 1H), 9.26 (s, 1H), 8.95 (s, 2H), 8.93 (s, 2H), 8.90 (d, ^3J = 5.3 Hz, 1H), 8.79 (d, ^3J = 5.3 Hz, 1H), 8.23 (br m, 10H), 7.90 (d, ^3J = 7.6 Hz, 2H), 7.78 (b m, 10H), 7.69 (d, ^3J = 6.0 Hz, 2H), 7.55 (d, ^3J = 8.3 Hz, 2H), 7.40 (d, ^3J = 8.3 Hz, 2H). UV−vis (toluene): λ_{max} (nm) (ε) = 333 (39 300), 436 (220 800), 559 (17 400), 594 (9100 mol^{-1} dm^3 cm^{-1}).

ZnP−Oligo-PPE_3−CHO (Zn6b). Yield: 95%. MS (MALDI): *m*/*z* 1005 [M^+]. ^{1}H NMR (300 MHz, $CDCl_3$): δ (ppm) 10.04 (s, 1H), 9.26 (s, 1H), 8.95 (s, 2H), 8.93 (s, 2H), 8.90 (d, ^3J = 5.3 Hz, 1H), 8.80 (d, ^3J = 5.3 Hz, 1H), 8.24 (br m, 10H), 7.90 (d, ^3J = 8.3 Hz, 2H), 7.78 (b m, 10H), 7.71 (br d, ^3J = 8.3 Hz, 2H), 7.58 (s, 4H), 7.53 (d, ^3J = 8.3 Hz, 2H), 7.39 (d, ^3J = 8.3 Hz, 2H). UV−vis (toluene): λ_{max} (nm) (ε) = 345 (60 000), 436 (298 000), 559 (24 300), 594 (12 700 mol^{-1} dm^3 cm^{-1}).

ZnP−Oligo-PPE_2−C_{60} (Zn7a). Yield: 97%. MS (MALDI): *m*/*z* 1652 [M^+], 932 [M − 720]$^+$, 720 [M − 932]$^+$. ^{1}H NMR (300 MHz, $CDCl_3$): δ (ppm) 9.26 (s, 1H), 8.94 (s, 2H), 8.91 (s, 2H), 8.88 (d, ^3J = 4.5 Hz, 1H), 8.77 (d, ^3J = 4.5 Hz, 1H), 8.19 (br m, 10H), 7.80−7.64 (series of broadened multiplets, 14H), 7.48 (d, ^3J = 8.3 Hz, 2H), 7.39 (d, ^3J = 8.3 Hz, 2H), 4.83 (d, ^2J = 9.8 Hz, 1H), 4.68 (s, 1H), 4.04 (d, ^2J = 9.8 Hz, 1H), 2.79 (s, 3H). UV−vis (toluene): λ_{max} (nm) (ε) = 324 (68 100), 436 (235 000), 559 (21 600), 594 (11 500 mol^{-1} dm^3 cm^{-1}).

ZnP−Oligo-PPE_3−C_{60} (Zn7b). Yield: 96%. MS (MALDI): *m*/*z* 1752 [M^+], 1032 [M − 720]$^+$, 720 [M − 1032]$^+$. ^{1}H NMR (300 MHz, $CDCl_3$): δ (ppm) 9.27 (s, 1H), 8.94 (s, 2H), 8.91 (s, 2H), 8.88 (d, ^3J = 4.5 Hz, 1H), 8.77 (d, ^3J = 4.5 Hz, 1H), 8.19 (br m, 10H), 7.80−7.63 (series of broadened multiplets, 14H),

7.57 (d, $^3J = 8.3$ Hz, 2H), 7.50 (d, $^3J = 7.5$ Hz, 4H), 7.40 (d, $^3J = 8.3$ Hz, 2H), 4.85 (d, $^2J = 9.8$ Hz, 1H), 4.70 (s, 1H), 4.06 (d, $^2J = 9.8$ Hz, 1H), 2.79 (s, 3H). UV−vis (toluene): λ_{max} (nm) (ε) = 333 (96 100), 436 (281 000), 559 (23 800), 594 (12 900 mol^{-1} dm^3 cm^{-1}).

Acknowledgment. This work was supported by the Deutsche Forschungsgemeinschaft DFG (SFB 583: Redoxaktive Metallkomplexe—Reaktivitätssteuerung durch molekulare Architektur), the FCI, and the Office of Basic Energy Sciences of the U.S. Department of Energy.

Supporting Information Available: UV−vis, ^{1}H NMR, FAB MS and MALDI-TOF MS spectra, and cyclic voltammetry results. This material is available free of charge via the Internet at http://pubs.acs.org.

References and Notes

(1) (a) Wasielewski, M. R. *Chem. Rev.* **1992**, *92*, 435–461. (b) Jordan, P.; Fromme, P.; Witt, H. T.; Klukas, O.; Saenger, W.; Krauss, N. *Nature* **2001**, *411*, 909–917. (c) Ben-Shem, A.; Frolow, F.; Nelson, N. *Nature* **2003**, *426*, 630–635. (d) Liu, Z.; Yan, H.; Wang, K.; Kuang, T.; Zhang, J.; Gui, L.; An, X.; Chang, W. *Nature* **2004**, *428*, 287–292.

(2) (a) Nelson, N.; Ben-Shem, A. *Nat. Rev.* **2004**, *5*, 1–12. (b) Zinth, W.; Wachtveitl, J. *ChemPhysChem* **2005**, *6*, 871–880. (c) Ivashin, N.; Larsson, S. *J. Phys. Chem. B* **2005**, *109*, 23051–23060. (d) Ziolek, M.; Pawlowicz, N.; Naskrecki, R.; Dobek, A. *J. Phys. Chem. B* **2005**, *109*, 18171–18176. (e) Kirmaier, C.; Holten, D. *Biochemistry* **1991**, *30*, 609–613. (f) Lauterwasser, C.; Finkele, U.; Scheer, H.; Zinth, W. *Chem. Phys. Lett.* **1991**, *183*, 471–477. (g) Holzapfel, W.; Finkele, U.; Kaiser, W.; Oesterhelt, D.; Scheer, H.; Stilz, H. U.; Zinth, W. *Chem. Phys. Lett.* **1989**, *160*, 1–7.

(3) (a) Schwab, P. F. H.; Levin, M. D.; Michl, J. *Chem. Rev.* **1999**, *99*, 1863–1933. (b) Creager, S.; Yu, C. J.; Bamdad, C.; O'Connor, S.; MacLean, T.; Lam, E.; Chong, Y.; Olsen, G. T.; Luo, J.; Gozin, M.; Kayyem, J. F. *J. Am. Chem. Soc.* **1999**, *121*, 1059–1064. (c) Segura, J. L.; Martin, N. *J. Mater. Chem.* **2000**, *10*, 2403–2435. (d) Kertesz, M.; Choi, C. H.; Yang, S. *Chem. Rev.* **2005**, *105*, 3448–3481. (e) Weder, C. *Chem. Commun.* **2005**, 5378–5389. (f) Benniston, A. C.; Harriman, A.; Rewinska, D. B.; Yang, S.; Zhi, Y. G. *Chem. Eur. J.* **2007**, *13*, 10194–10203.

(4) (a) Marcus, R. A.; Sutin, N. *Biochim. Biophys. Acta* **1985**, *811*, 265–322. (b) Marcus, R. A. *Annu. Rev. Phys. Chem.* **1964**, *15*, 155–196. (c) Newton, M. D.; Sutin, N. *Annu. Rev. Phys. Chem.* **1984**, *35*, 437–480. (d) Bolton, J. R.; Mataga, R.; McLendon, G. *Advances in Chemistry Series CSC Symposium Series*; American Chemical Society and Canadian Society for Chemistry; Oxford University Press: New York, 1991; Chapter 3.

(5) (a) Winters, M. U.; Pettersson, K.; Mårtensson, J.; Albinsson, B. *Chem. Eur. J.* **2005**, *11*, 562–573. (b) Pettersson, K.; Kyrychenko, A.; Rönnow, E.; Ljungdahl, T.; Mårtensson, J.; Albinsson, B. *J. Phys. Chem. A* **2006**, *110*, 310–318. (c) Eng, M. P.; Albinsson, B. *Angew. Chem., Int. Ed.* **2006**, *45*, 5626–5629.

(6) (a) Van Hal, P. A.; Meskers, S. C. J.; Janssen, R. A. J. *Appl. Phys. A: Mater. Sci. Process.* **2004**, *79*, 41–46. (b) Giacalone, F.; Segura, J. L.; Martin, N.; Ramey, J.; Guldi, D. M. *Chem. Eur. J.* **2005**, *11*, 4819–4834. (c) De la Torre, G.; Giacalone, F.; Segura, J. L.; Martin, N.; Guldi, D. M. *Chem. Eur. J.* **2005**, *11*, 1267–1280. (d) Figueira-Duarte, T. M.; Gégout, A.; Nierengarten, J. F. *Chem. Commun.* **2007**, 109–119. (e) Toivonen, T. L. J.; Hukka, T. I. *J. Phys. Chem. A* **2007**, *111*, 4821–4828.

(7) (a) Nierengarten, J. F.; Gu, T.; Aernouts, T.; Geens, W.; Poortmans, J.; Hadziioannou, G.; Tsamouras, D. *Appl. Phys. A: Mater. Sci. Process.* **2004**, *79*, 47–49. (b) Koynov, K.; Bahtiar, A.; Bubeck, C.; Mühling, B.; Meier, H. *J. Phys. Chem. B* **2005**, *109*, 10184–10188. (c) Chaignon, F.; Torroba, J.; Blart, E.; Borgström, M.; Hammarström, L.; Odobel, F. *New J. Chem.* **2005**, *29*, 1272–1284. (d) Zhao, Y.; Shirai, Y.; Slepkov, A. D.; Cheng, L.; Alemany, L. B.; Sasaki, T.; Hegmann, F. A.; Tour, J. M. *Chem. Eur. J.* **2005**, *11*, 3643–3658. (e) Atienza, C.; Martìn, N.; Wielopolski, M.; Haworth, N.; Clark, T.; Guldi, D. M. *Chem. Commun.* **2006**, 3202–3204. (f) Wielopolski, M.; Atienza, C.; Clark, T.; Guldi, D. M.; Martìn, N. *Chem. Eur. J.* **2008**, *14*, 6379–6390. (g) Fortage, J.; Göransonn, E.; Blart, E.; Becker, H. C.; Hammarström, L.; Odobel, F. *Chem. Commun.* **2007**, 4629–4631. (h) Pu, K. Y.; Qi, X. Y.; Yang, Y. L.; Lu, X. M.; Li, T. C.; Fan, Q. L.; Whang, C.; Liu, B.; On Chan, H. S.; Huang, W. *Chem. Eur. J.* **2008**, *14*, 1205–1215.

(8) (a) Vail, S. A.; Krawczuk, P. J.; Guldi, D. M.; Palkar, A.; Echegoyen, L.; Tomé, J. P. C.; Fazio, M. A.; Schuster, D. I. *Chem. Eur. J.* **2005**, *11*, 3375–3388. (b) Vail, S. A.; Schuster, D. I.; Guldi, D. M.; Isosomppi, M.; Tkachenko, N.; Lemmetyinen, H.; Palkar, A.; Echegoyen, L.; Chen, X.; Zhang, J. Z. H. *J. Phys. Chem. B* **2006**, *110*, 14155–14166. (c) Yamanaka, K.; Fujitsuka, M.; Araki, Y.; Tashiro, K.; Sato, A.; Yuzawa, T.; Aida, T. *J. Porphyrins Phthalocyanines* **2007**, *11*, 397–405.

(9) (a) Nakamura, T.; Fujitsuka, M.; Araki, Y.; Osamu, I.; Ikemoto, J.; Takimiya, K.; Aso, Y.; Otsubo, T. *J. Phys. Chem. B* **2004**, *108*, 10700–10710. (b) Huang, C. H.; McClenaghan, N. D.; Kuhn, A.; Hofstraat, J. W.; Bassani, D. M. *Org. Lett.* **2005**, *7*, 3409–3412. (c) Petrella, A.; Cremer, J.; De Cola, L.; Bäuerle, P.; Williams, R. M. *J. Phys. Chem. A* **2005**, *109*, 11687–11695. (d) Sivula, K.; Luscombe, C. K.; Thompson, B. C.; Fréchet, J. M. J. *J. Am. Chem. Soc.* **2006**, *128*, 13988–13989. (e) Narutaki, M.; Takimiya, K.; Otsubo, T.; Harima, Y.; Zhang, H.; Araki, Y.; Osamu, I. *J. Org. Chem.* **2006**, *71*, 1761–1768.

(10) (a) Barigelletti, F.; Flamigni, L.; Guardigli, M.; Juris, A.; Beley, M.; Chodorowski-Kimmes, S.; Collin, J.-P.; Sauvage, J.-P. *Inorg. Chem.* **1996**, *35*, 136–142. (b) Berresheim, A. J.; Müller, M.; Müllen, K. *Chem. Rev.* **1999**, *99*, 1747–1785. (c) Schlicke, B.; Belser, P.; De Cola, L.; Sabbioni, E.; Balzani, V. *J. Am. Chem. Soc.* **1999**, *121*, 4207–4214. (d) Helms, A.; Heiler, D.; McLendon, G. *J. Am. Chem. Soc.* **1992**, *114*, 6227–6238. (e) Cohen, R.; Stokbro, K.; Martin, J. M. L.; Ratner, M. A. *J. Phys. Chem. C* **2007**, *111*, 14893–14902.

(11) Winters, M. U.; Dahlstedt, E.; Blades, H. E.; Wilson, C. J.; Frampton, M. J.; Anderson, H. L.; Albinsson, B. *J. Am. Chem. Soc.* **2007**, *129*, 4291–4297.

(12) Pettersson, K.; Wiberg, J.; Ljungdahl, T.; Mårtensson, J.; Albinsson, B. *J. Phys. Chem. A* **2006**, *110*, 319–326.

(13) (a) Xiao, X.; Nagahara, L. A.; Rawlett, A. M.; Tao, N. *J. Am. Chem. Soc.* **2005**, *127*, 9235–9240. (b) Lewis, P. A.; Inman, C. E.; Maya, F.; Tour, J. M.; Hutchinson, J. E.; Weiss, P. S. *J. Am. Chem. Soc.* **2005**, *127*, 17421–17426. (c) Huber, R.; Gonzalez, M. T.; Wu, S.; Langer, M.; Grunder, S.; Horhoiu, V.; Mayor, M.; Bryce, M. R.; Wang, C.; Jitchati, R.; Schönenberger, C.; Calame, M. *J. Am. Chem. Soc.* **2008**, *130*, 1080–1084.

(14) (a) Fan, F.-R. F.; Lai, R. Y.; Cornil, J.; Karzazi, Y.; Brédas, J. L.; Cai, L.; Cheng, L.; Yao, Y.; Price, D. W., Jr.; Dirk, S. M.; Tour, J. M.; Bard, A. J. *J. Am. Chem. Soc.* **2004**, *126*, 2568–2573. (b) Zangmeister, C. D.; Robey, S. W.; van Zee, R. D.; Yao, Y.; Tour, J. M. *J. Am. Chem. Soc.* **2004**, *126*, 3420–3421. (c) Fan, F.-R. F.; Yao, Y.; Cai, L.; Cheng, L.; Tour, J. M.; Bard, A. J. *J. Am. Chem. Soc.* **2004**, *126*, 4035–4042.

(15) Meier, H.; Mühling, B.; Kolshorn, H. *Eur. J. Org. Chem.* **2004**, *103*, 3–1042.

(16) (a) Gholap, A. R.; Venkatesan, K.; Pasricha, R.; Daniel, T.; Lahoti, R. J.; Srinivasan, K. V. *J. Org. Chem.* **2005**, *70*, 4869–4872. (b) Liang, Y.; Xie, Y. X.; Li, J. H. *J. Org. Chem.* **2006**, *71*, 379–381. (c) Chinchilla, R.; Najera, C. *Chem. Rev.* **2007**, *107*, 874–922.

(17) Maggini, M.; Scorrano, G.; Prato, M. *J. Am. Chem. Soc.* **1993**, *115*, 9798–9799.

(18) (a) Austin, W. B.; Bilow, N.; Kelleghan, W. J.; Lau, K. S. Y. *J. Org. Chem.* **1981**, *46*, 2280–2286. (b) Thorand, S.; Krause, N. *J. Org. Chem.* **1998**, *63*, 8551–8553.

(19) Yao, Y.; Tour, J. M. *J. Org. Chem.* **1999**, *64*, 1968–1971.

(20) Lembo, A.; Tagliatesta, P.; Guldi, D. M. *J. Phys. Chem. A* **2006**, *111*, 11424–11434.

(21) Noteworthy, the reduction process is not reproducible once passing the first scan. A side reaction at the working electrode−solution interface generates adsorbed films on the electrode surface, which requires removal prior to continuing the measurements. It is plausible to suppose that the aldehyde group is involved in these side reactions.

(22) Wielopolski, M.; Atienza-Castellanos, A.; Clark, T.; Guldi, D. M.; Martin, N. *Chem. Eur. J.* **2008**, *14*, 6379–6390.

(23) Clark T.; Alex A.; Beck B.; Burkhardt F.; Chandrasekhar J.; Gedeck P.; Horn A. H. C.; Hutter M.; Martin B.; Rauhut G.; Sauer W.; Schindler T.; Steinke T. VAMP 10.0; Erlangen, Germany, 2003.

(24) Winget, P.; Horn, A. H. C.; Selcuki, C.; Martin, B.; Clark, T. *J. Mol. Model.* **2003**, *9*, 408–414.

(25) (a) Becke, A. D. *J. Chem. Phys.* **1993**, *98*, 5648. (b) Burke, K.; Perdew, J. P.; Wang, Y. In *Electronic Density Functional Theory: Recent Progress and New Directions*; Dobson, J. F., Vignale, G., Das, M. P., Eds.; Plenum: New York, 1998.

(26) Frisch, M. J.; Trucks, G. W.; Schlegel, H. B.; Scuseria, G. E.; Robb, M. A.; Cheeseman, J. R.; Montgomery, J. A., Jr.; Vreven, T.; Kudin, K. N.; Burant, J. C.; Millam, J. M.; Iyengar, S. S.; Tomasi, J. J.; Barone, V.; Mennucci, B.; Cossi, M.; Scalmani, G.; Rega, N.; Petersson, G. A.; Nakatsuji, H.; Hada, M.; Ehara, M.; Toyota, K.; Fukuda, R.; Hasegawa, J.; Ishida, M.; Nakajima, T.; Honda, Y.; Kitao, O.; Nakai, H.; Klene, M.; Li, X.; Knox, J. E.; Hratchian, H. P.; Cross, J. B.; Adamo, C.; Jaramillo, J.; Gomperts, R.; Stratmann, R. E.; Yazyev, O.; Austin, A. J.; Cammi, R.; Pomelli, C.; Ochterski, J. W.; Ayala, P. Y.; Morokuma, K.; Voth, A.; Salvador, P.; Dannenberg, J. J.; Zakrzewski, V. G.; Dapprich, S.; Daniels, A. D.; Strain, M. C.; Farkas, O.; Malick, D. K.; Rabuck, A. D.; Raghavachari, K.; Foresman, J. B.; Ortiz, J. V.; Cui, Q.; Baboul, A. G.; Clifford, S.; Cioslowski, J.; Stefanov, B. B.; Liu, G.; Liashenko, A.; Piskorz, P.; Komaromi, I.; Martin, R. L.; Fox, D. J.; Keith, T.; Al-Laham, M. A.; Peng, C. Y.; Nanayakkara, A.; Challacombe,

M.; Gill, P. M. W.; Johnson, B.; Chen, W.; Wong, M. W.; Gonzalez, C.; Pople, J. A. Gaussian 03, revision D.02; Gaussian, Inc.: Wallingford, CT, 2004.

(27) (a) James, P. V.; Sudeep, P. K.; Suresh, C. H.; Thomas, K. G. *J. Phys. Chem. A* **2006**, *110*, 4329–4337. (b) Levitus, M.; Schmieder, K.; Ricks, H.; Shimizu, K. D.; Bunz, U. H. F.; Garcia-Garibay, M. A. *J. Am. Chem. Soc.* **2002**, *124*, 8181–8181. (c) Schmieder, K.; Levitus, M.; Dang, H.; Garcia-Garibay, M. A. *J. Phys. Chem. A* **2002**, *106*, 1551–1556. (d) Sudeep, P. K.; James, P. V.; Thomas, K. G.; Kamat, P. V. *J. Phys. Chem. A* **2006**, *110*, 5642–5649. (e) Eng, M. P.; Martensson, J.; Albinsson, B. *Chem. Eur. J.* **2008**, *14*, 2819–2826.

(28) Calculated energies in vacuum are higher due to a lack of solvent stabilization.

(29) (a) Clark, T.; Lin, Jr.-H.; Horn, A. H. C. Parasurf 07; Cepos InSilico Ltd.: Ryde, U.K., 2007; www.ceposinsilico.com. (b) Ehresmann, B.; Martin, B.; Horn, A. H. C.; Clark, T. *J. Mol. Model.* **2003**, *9*, 342–348. (c) Clark, T. *J. Mol. Graphics Modell.* **2004**, *22*, 519–525.

(30) Lanig, H.; Koenig, R.; Clark, T. Tramp 1.1d.; University of Erlangen, Erlangen, Germany, 2005.

(31) Weller, A. Z. *Phys. Chem. (Munich)* **1982**, *133*, 93–98.

(32) Ventura, B.; Flamigni, L.; Marconi, G.; Lodato, F.; Officer, D. L. *New J. Chem.* **2008**, *32*, 166–178.

JP809557E